Review Article

Hongling Tian*, Sihan Ma and Deng Long

Emerging nanocarriers: rational design and biomedical application

https://doi.org/10.1515/revic-2025-0019
Received March 17, 2025; accepted June 12, 2025;
published online June 26, 2025

Abstract: Nanosystems, renowned for their remarkable physical and chemical attributes arising from their unique morphology and structure, such as elevated specific surface areas, pronounced macroscopic quantum effects, distinctive dielectric properties, and notable small size effects, are poised to transform cancer treatment paradigms by potentially supplanting conventional chemical drugs. This revolutionary potential has generated significant buzz and attracted considerable interest within the medical diagnostics and therapeutics landscape. Extensive research has underscored the exceptional capabilities of nano-scale diagnostic agents, which have been extensively employed in imaging and anti-tumor applications, heralding a promising horizon for their utilization. This review endeavors to offer an exhaustive synthesis of the latest research strides in nanomedical theranostic candidates. It delves into the design strategies and prospective applications of various nanomaterials within the domains of tumor therapy and imaging, aiming to furnish valuable perspectives and directives for the future trajectory of nanomedicine. Specifically, the review meticulously explores and elucidates methodologies for enhancing tumor elimination through the judicious modification of nanomaterials. Furthermore, this work meticulously discusses the formidable challenges and intricacies associated with the development of optimal therapeutic nanomaterials, as well as the hurdles impeding their clinical translation. The overall aim is to advance the application and development of nanomaterials for effective and precise collaborative diagnosis and treatment of disease.

***Corresponding author: Hongling Tian**, Changde Hospital, Xiangya School of Medicine, Central South University (The First People's Hospital of Changde City), Changde 415000, China, E-mail: thl2271404307@163.com
Sihan Ma and Deng Long, College of Big Data and Information Engineering, Guizhou University, Guiyang 550025, China. https://orcid.org/0000-0001-9684-0909 (S. Ma)

Keywords: nanomedicine; theranostic applications; design approach; modification

1 Introduction

Accurate diagnosis and treatment of tumor diseases have always been a crucial objective pursued by the medical field, as it can save valuable time and costs, capitalize on the critical treatment window, alleviate patient discomfort, and foster the healthy progress of society.[1] In pursuit of this objective, researchers across various disciplines have devoted considerable time and energy to the investigation of innovative technologies and approaches. It is widely acknowledged that conventional clinical cancer therapies, such as surgical intervention, radiotherapy, and chemotherapy, are not without their constraints. Regrettably, these approaches pose risks such as harming normal cells, undermining the immune system, and elevating the recurrence rate of cancers.[2–4] With the swift advancement of science and technology, the emergence of nanomaterials has heralded a new era of precision diagnosis and treatment, effectively addressing these shortcomings. These nanomaterials are extensively employed in the realm of medical oncology, garnering widespread attention and yielding satisfactory outcomes.[5]

Currently, the main nanomaterials for anticancer strategies include radiotherapy (RT),[6] photothermal therapy (PTT),[7–12] photodynamic therapy (PDT),[13–15] sonodynamic therapy (SDT)[16–18] and emerging gastherpay (GT).[19,20] RT employs high energy X-ray/ion beam to carry out cell killing by radioactive energy transfer. PTT achieves cell death mainly through effective photothermal conversion by light irradiation, the temperature above 50 °C can achieve good therapeutic effect.[10] PDT performs anticancer activity by employing reactive oxide species (ROS) induced by light irradiation. SDT is similar with PDT, the light irradiation is replaced by ultrasound. Interestingly, GT can generate the poisonous gas to damage cells under external action. Due to the unique advantages of these therapeutic modalities, nanomaterials with different therapeutic capabilities have been continuously developed in recent years.

Furthermore, achieving convenient and rapid tumor diagnosis poses a significant challenge to the realm of

precision medicine, which aims to deliver swift and well-reasoned treatment plans tailored to cancer patients. In clinical practice, X-ray computed tomography (CT) and magnetic resonance imaging (MRI) with the advantages of non-invasive, high intensity penetration depth, real-time 3D tomography acquisition capabilities are the two most common diagnostic methods and can provide detailed anatomical image information.[21] In the process of using these imaging techniques, it is easy to cause the loss of image information when processing anatomical information due to the particularity of soft tissue or lesions. Therefore, most cases require the use of clinical contrast agents (CAs) for image information enhancement. However, most clinical contrast agents are mostly small molecule drugs, although they can achieve good image signal enhancement, body fluid cycle is short due to its small molecule characteristics, and easy to be rapidly metabolized, generally require a large amount or continuous injection, which will inevitably cause side effects.[22] Nanomaterials can effectively prolong the blood circulation time, and high atomic number aggregation can achieve better ray attenuation and relaxation ability.[23–25] Thus, employing nanomaterials as imaging contrast agents (CAs) holds promise for generating clearer image data, thereby offering invaluable insights for the precise diagnosis of diseases.

Recently, a variety of nanomaterials have been reported to achieve the theranostic application of tumor, further extending our horizons. Although these reports presented good pre-clinical capabilities, a comprehensive overview and systematic classification of nanomaterial theranostic agents (TAs) are still insufficient. A critical aspect that has been hitherto underexplored is how to enhance the therapeutic efficacy of nanomaterials to fully harness their potential. In this context, the present work undertakes a comprehensive review of the advancements in nanomaterial research concerning the diagnosis and treatment of cancer. It encapsulates the applications of diverse nanomaterial types in both diagnostic and therapeutic domains, alongside a succinct overview of their antitumor mechanisms and factors influencing imaging efficacy (as depicted in Scheme 1). Crucially, the work delves deeper into the pivotal factors that can be manipulated to augment the diagnostic and therapeutic performance of nanomaterials, thereby serving as a cornerstone for the development of more potent nanomaterial-based interventions.

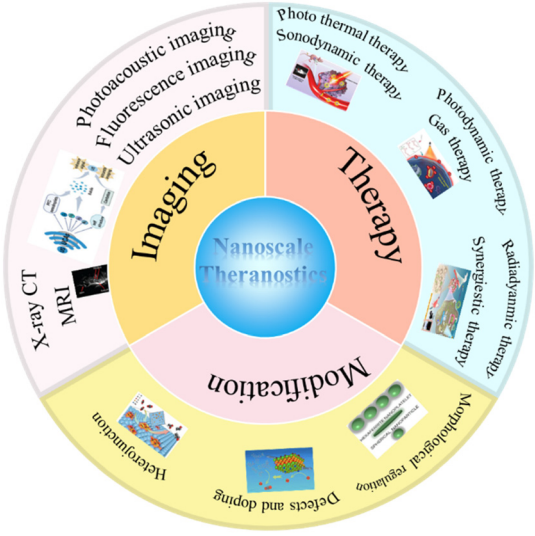

Scheme 1: Classification and application of nanoscale theranostic agents.

2 Classification of nanomaterials

Briefly, nanomaterials can be classified as organic and inorganic materials. Inorganic compounds are mainly composed of inorganic elements, in nature known elements, in addition to hydrocarbon oxygen and other gas elements, most can be divided into inorganic components. Inorganic nanomaterials are also the most widely used. Specifically, by compounds that can be divided into different elemental bases. For instance, bismuth-based nanomaterials,[26–30] iron-based nanomaterials,[31–35] gadolinium-based nanomaterials[36–40] etc. Organic compounds do not contain inorganic elements and are mainly composed of elements such as carbon, hydrogen and oxygen etc. For example, polymers,[41–46] ionic liquid derivatives,[47,48] phosphorus[49–52] etc. The morphologic classification can be divided into nanomaterials with one dimensional (1D), two dimensional (2D) and three dimensional (3D) structures. Nanomaterials with a special structural orientation can perform different functions, such as 0D nanomaterials mainly include quantum dots, nanoparticles and nanoclusters, due to their unique optical and electronic properties, 0D nanomaterials have been widely used in optoelectronics and biomarkers. In the meantime, 0D nanomaterials can achieve photoexcited luminescence and good kidney clearance;[27,53] 1D nanofibers/nanotubes have a porous structure, higher specific surface area and volume ratio, and unique physicochemical properties;[9] 2D nanomaterials can achieve good surface drug loading ability and modification due to their ultra-thin nanostructure, large specific surface area;[54,55] 3D nanomaterials are the most common and pervasive, with high specific surface area, good biocompatibility and controllable pore size, and have important applications in the fields of drug carriers and biomedical imaging.[26] Different shapes and sizes can be effectively regulated during the preparation process, and the creation of nanomaterials of different dimensions through different synthesis methods can provide

Table 1: Overview of nanomaterials with different morphologies and sizes.

Materials	Morphology	Type	Size	Application	Ref
GNBPs	1D	Inorganic	137 × 22 nm	OCT	56
Fe_2O_3@BSA	0D	Inorganic	3.47 nm	MRI	31
BGQDs	0D	Organic	4.6 nm	MRI	57
ZnO	0D	Inorganic	5.7 nm	Therapy	58
CeO_2	0D	Inorganic	4.8 nm	CT	59
SBBHs	3D	Inorganic	–	CT	60
Carbon dots	0D	Organic	4.7 nm	MRI	61
Fe_3O_4/MnO	3D	Inorganic	20 nm	MRI	62
$NaLuF_4$:Yb/Gd/Er	1D	Inorganic	–	OCT	63
Pd nanomaterials	2D	Inorganic	21–51 nm	PA	54
MIONCs	3D	Inorganic	80–100 nm	Theranostic	64
BSO–FeS_2	0D	Inorganic	7.27 nm	Theranostic	65
TiO_{1+x}	1D	Inorganic	1.8 × 28.6 nm	Theranostic	66
CoFe-LDH	2D	Inorganic	200 nm	Theranostic	67
MnO_2	3D	Inorganic	116/128 nm	Theranostic	68
SnS_2	3D	Inorganic	500 nm	Therapy	69
FeS_2@C-ICG-PEG	3D	Inorganic	200 nm	Theranostic	70
BiOCl	2D	Inorganic	150–250 nm	Theranostic	71

GNBPs: gold nanobipyramids. OCT: optical coherence tomography. BGQDs: boron-doped graphene quantum dots. SBBHs: SP–Bi biohybrids. PA: photoacoustic imaging. MIONCs: hollow magnetic nanoclusters.

effective methodological support for precise diagnosis and treatment. In order to deepen the understanding of nanomaterials with different morphology, a summary of nanomaterials with different morphology is provided in Table 1.

3 Synthesis methods of nanomaterials

The synthesis approach employed for nanomaterials exerts a profound influence on both their morphology and physicochemical attributes. By finely tuning parameters such as morphology, size, crystal phase, and surface properties, diverse synthesis techniques can significantly modulate the mechanical, optical, electrical, magnetic, and catalytic performances of these materials. Alterations in their physical and chemical properties, coupled with morphological transformations, hold immense potential for enhancing the precision of disease diagnosis and treatment strategies. Consequently, strategic selection of an appropriate synthesis method is pivotal for the fabrication of nanomaterials with desired characteristics, thereby facilitating their application in advanced precision medicine.

3.1 Hydro/solvothermal fabrication

As a well-established nanomaterial synthesis technique, the hydrothermal method primarily involves inducing atomic nucleation and crystallization under specific temperature and pressure conditions, followed by precipitation from the resultant mixture. Miaomiao Yuan et al. synthesized porous Co_3O_4 nanoplates by using hydrothermal strategy for performing highly efficient tumor killing.[72] The morphology of the synthesized Co_3O_4 nanomaterials was observed by TEM (Figure 1a), suggesting a porous structure. HRTEM images showed lattice fringes with interfacial spacing of approximately 0.243 nm, corresponding to the (311) plane of standard Co_3O_4 (Figure 1b). Meanwhile, the results also verified the good crystallization. Similarly, Guannan Zhu et al. used hydrothermal strategy to fabricate the $GdVO_4$:Eu^{3+}, Bi^{3+} nanoparticles for bioimaging application.[37] The synthesized nanomaterial has a tetragonal-phase $GdVO_4$ structure, and showed a stable crystal structure (Figure 1c). Importantly, during the hydrothermal synthesis process, pH of the system has a significant effect on the morphology of the synthetic system, which played a key role in biomedical applications. Ziming Cui et al. achieved the synthesis of different Bi_2WO_6 materials by adjusting the pH in the reaction environment.[73] As a result, when the pH of the reaction system is acidic, the morphology of the prepared samples mainly presents flower-like structures. When the pH is 7, a large number of sheet structures are produced. When the pH is more alkaline, the synthesized Bi_2WO_6 nanomaterials are transformed into irregular flake-like structures (Figure 1d). In addition, surface coating also influenced the morphology of nanomaterials. Bi_2Te_3 nanoparticles of varying sizes were prepared by using the surfactants including ethylene glycol, polyethylpyrodanone (PVP) and ethylenediamine tetraacetic

acid.[74] Thus, reasonable adjustment of pH and surface activator during hydrothermal reaction can achieve satisfactory preparation of nanomaterials. Solvothermal is similar to hydrothermal synthesis, with the key distinction being the substitution of water with an organic liquid as the primary solvent. Yuanchun Si et al. employed solvothermal method to synthesize the gadolinium-doped iron oxide nanoclusters ($HSiO_2$@GdIONC).[75] The target product was prepared by a three-step synthesis method. The first step was to prepare the GdIONC core, and the core structure was prepared by heating at 270 °C in PVP-EG mixed solution. Subsequently, the outer shell is wrapped and SiO_2 was used as the shell structure. Finally, the SiO_2@GdIONC was collected by magnetic separation and wash three times with distilled water (Figure 1e). In total, the required material synthesis process

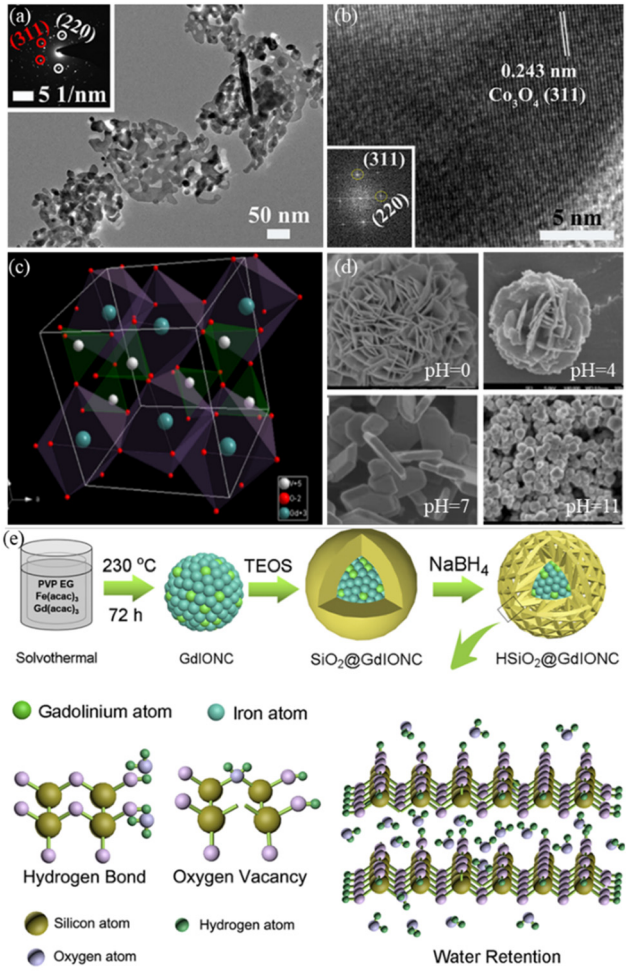

Figure 1: Synthesis and morphological characterization. (a) TEM image of Co_3O_4. (b) HRTEM image of Co_3O_4[72]. Copyright 2020, Elsevier. (c) Schematic illustration of the as-prepared $GdVO_4$:Eu^{3+}, Bi^{3+} structure.[37] Copyright 2019, American Chemical Society. (d) SEM images of Bi_2WO_6 nanomaterials under different pH reaction system.[73] Copyright 2016, Springer Link. (e) Solvothermal fabrication of $HSiO_2$@GdIONC.[75] Copyright 2019, Elsevier.

can be realized through the reasonable coordination of water and organic solvent. Importantly, because the size and morphology of synthetic nanomaterials significantly affect their physicochemical properties, the ability to prepare morphologically controllable nanomaterials is critical.[76]

3.2 Microwave fabrication

Microwave synthesis primarily leverages microwave radiation for energy transfer, enabling substances to absorb microwave energy and undergo thermal energy conversion. This process facilitates the synthesis of organic/inorganic materials during heating, offering notable advantages such as rapid reaction rates, uniform heating, and high selectivity. Xiaoyang Wang et al. constructed BiOBr nanomaterials by employing microwave technique.[77] The synthesis temperature was controlled by adjusting the microwave irradiation time, and the generation of BiOBr nanomaterials with different sizes was realized by adjusting the concentration of precursors. The results showed that the concentration of precursors and the microwave irradiation temperature had important effects on the energy band gap of BiOBr nanomaterials.[78] Xinhua Zhu et al. prepared single crystal perovskite type nanocrystals by microwave-assisted hydrothermal method, which were microwave reacted for 60 min at 180 °C, and then cooled to room temperature.[79] The final products were collected by centrifugation and dried to obtain the product powders. In this process, the utilization of microwave and hydrothermal method can effectively regulate the particle morphology and size distribution. In addition, large-scale products can be easily synthesized using microwave-assisted methods. The operation is both convenient and straightforward, while also mitigating the safety risks associated with the high-temperature and high-pressure conditions required in hydrothermal methods.

3.3 Reduction-coprecipitation fabrication

During the reaction, a reagent with redox activity can be added to achieve rapid reaction to prepare nanomaterials, which has the advantage of fast and efficient. Among reducing agents, the most commonly used representative is sodium borohydride ($NaBH_4$). Maryam Hosseini et al. employed $NaBH_4$ to carry out the fabrication of spirulina–bismuth biohybrids (SBBHs).[60] Dissolving $Bi(NO_3)_3{\cdot}5H_2O$ in an aqueous solution of HNO_3, then transfer it to a round-bottled flask and place it in a controlled temperature bath (40 °C). Spirulina powder was added into the mixture and mixed with the above solution, and then different proportions of $NaBH_4$ solution were added. Color changes were

observed during continuous addition, indicating that the mixture was reduced during the reaction process, and the reaction product SBBHs was obtained by further centrifuge washing and purification (Figure 2a). In addition to the use of reducing chemical reagents, the reduction activity of biological macromolecules can also be used to synthesize nanomaterials. Shuai Xu et al. used bovine serum albumin (BSA) to prepare magnetic Fe_2O_3@BSA nanomaterials (Figure 2b).[31] In this study, Fe_2O_3 was synthesized by BSA reduction precipitation method. Under N_2 protection and 37 °C water bath, the BSA solution was added to the iron salt solution, and then NaOH and hydrogen peroxide were injected to accelerate the Fe nucleation and growth. Finally, the obtained mixture underwent washing and drying procedures. The method was used by Pratap C. Naha et al. to prepare CeO_2 nanomaterials.[59] In the presence of dextran, CeO_2 nanoparticles were formed by adding ammonium hydroxide to precipitate cerium salt. In the meantime, the introduction of dextran on the CeO_2 surface enhanced the stability in phosphate-buffered saline (PBS). Sung Jun Park et al. used a facile co-precipitation method to prepare the Gd_2O_3:Pr^{3+} nanospheres.[38] The size of the synthesized nanomaterials varies with different reaction times. Using compounds with reducing groups to facilitate the growth and preparation of nanomaterials can often lead to time and cost savings. However, during the reduction process, there is a risk of agglomeration among smaller nanomaterials, which can ultimately decrease the yield of the final nanomaterial products.

3.4 Radiation methods

The fundamental principle underlying the synthesis of nanomaterials involves harnessing the high-energy characteristics of radioactive rays, particularly gamma rays and electrons, to initiate chemical reactions conducive to the production of nanoscale materials. Throughout the course of the reaction, these rays interact with the substance, giving rise to highly reactive species such as free radicals and ions.[80] These species subsequently participate in the chemical reaction, leading to alterations in the chemical composition and structural arrangement of the substance.[81] Sajid Ahmad et al. introduced the gamma radiation-assisted synthesis of polyaniline-based nanoparticles and nanocomposites.[82] It is suspected that the main advantage of irradiation is convenient delivery, and the pollution of secondary products is reduced to a certain extent compared with chemical methods. Junchang Chen et al. considered that electron energies are orders of magnitude higher than any chemical bond, and that many highly active substances can be supplied *in situ* by stable molecules under ionizing irradiation to significantly activate and accelerate synthesis. In addition, the radiation etching effect is present at the same time, which may be beneficial to enhance several properties such as catalysis and mass transfer. Therefore, they recently used irradiation by high-energy electron beams generated by industrial accelerators as a unique energy source to activate the formation reaction of Na-A molecular sieves.[83] In short, the effective use of radiation energy to achieve the preparation and growth of nanomaterials, can save energy and reduce chemical pollution, and then can achieve industrial grade preparation under appropriate circumstances, is a promising preparation method.

3.5 Other methods

In addition to the above more mainstream synthesis methods, some synthesis methods are also widely used in the

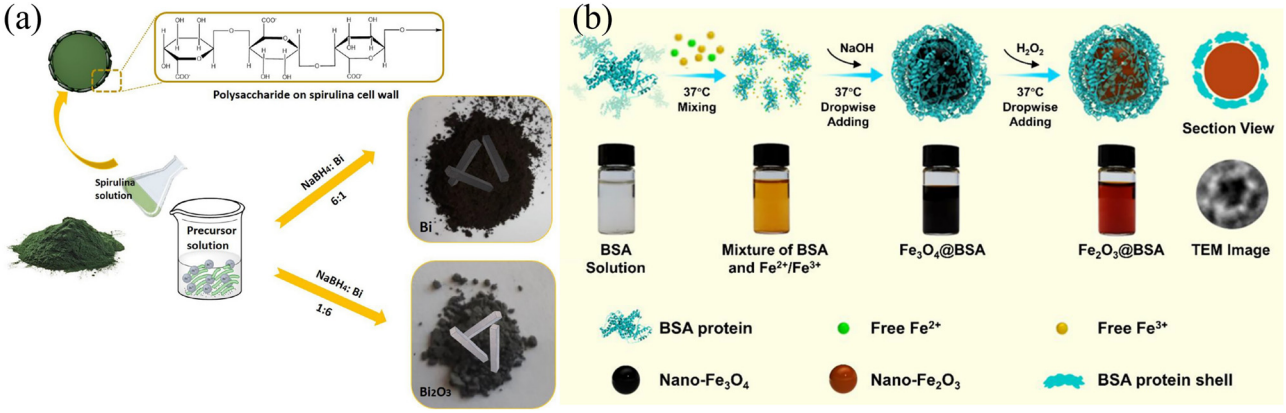

Figure 2: The synthetic pathways of nanomaterials. (a) Schematic illustration of the fabrication of spirulina–bismuth biohybrids.[60] Copyright 2020, American Chemical Society. (b) Illustration of the synthesis of Fe_2O_3 nanoparticles.[31] Copyright 2020, American Chemical Society.

synthesis of nanomaterials. For instance, the sol-gel method mainly uses compounds containing high chemical active components as precursors, and mixes these raw materials uniformly in the liquid phase, and carries out hydrolysis and condensation chemical reactions to form a stable transparent sol system in the solution. The sol slowly polymerizes between the aged colloidal particles to form a gel with a three-dimensional network structure, and the gel network is filled with the solvent that loses fluidity, forming a gel. The gel was dried and sintered to produce molecular and even nanostructured materials. Different nanoscale materials were constructed by the sol-gel method, reported by Maleki et al.[84] Zhang et al.[85] The microemulsion method uses two kinds of insoluble solvents to form emulsion under the action of surfactants, and nanoparticles are obtained by nucleation, coalescence, agglomeration and heat treatment in microbubbles. Cao et al. employed the microemulsion strategy to fabricate the various $BiVO_4$ composites,[86] providing an insightful view for the regulation synthesis of nanomaterials. Although the microemulsion method offers an effective approach for synthesizing nanomaterials with high purity by circumventing impurity contamination, it often comes with a substantial cost. Moreover, the relatively low activity and inadequate stability of emulsifiers during the preparation process can hinder the widespread application of this method. Vapor deposition represents a technological approach that leverages physical and chemical phenomena occurring in the gaseous phase to deposit a metal or compound coating, endowed with unique properties, onto the surface of a workpiece. Through the modification of the workpiece's surface composition, this method enables the fabrication of films featuring super-hard, wear-resistant layers or exhibiting exceptional optical and electrical characteristics. Vapor deposition technology is mainly divided into chemical vapor deposition (CVD) and physical vapor deposition (PVD). Long et al. used CVD to carry out the MoS_2 growth,[87] and the film was formed by chemical reaction of gaseous compounds or elements containing film elements on the substrate surface. The ball milling method is to grind the powder for a long time to achieve the preparation of micron or submicron particles. Alessandro Barge et al. performed an efficient, solvent-free synthesis of several organic molecules by using the energy generated by the mechanochemical activation of a planetary ball mill.[88] In general, choosing the appropriate synthesis method according to the actual situation is conducive to the synthesis of nanomaterials with high efficiency and good application. A thorough understanding of the synthesis strategies of various nanomaterials will help to select the most suitable method to prepare satisfactory nanomaterials.

4 Antitumor applications

4.1 Photothermal strategy

Photothermal therapy constitutes an innovative treatment modality that employs nanomaterials characterized by exceptional photothermal conversion efficiency. These nanomaterials are introduced into the body and subsequently directed to tumor tissues via targeted recognition technologies. Upon exposure to an external light source, typically near-infrared light, the nanomaterials convert light energy into thermal energy, thereby inducing the demise of cancer cells. The higher the photothermal conversion efficiency, the better the therapeutic effect can be achieved. In PTT, the most critical is the photothermal conversion efficiency, and high photothermal conversion efficiency means that more light energy is absorbed and utilized to achieve outstanding anti-tumor advantages. In general, surface modification to improve the efficiency of photothermal conversion is the most commonly used method. Different surface modification components play a different effect, which leads to different photothermal conversion efficiency. Li Wang et al. employed 2D CoFe-LDH nanosheets to perform highly efficient PTT for antitumor (Figure 3a).[67] The CoFe-500 was rapidly heated to ~ 70 °C under 808 nm laser irradiation, while the temperature of CoFe-LDH or PBS solution was negligible under laser illumination (Figure 3b). The results showed that the photothermal conversion efficiency (η) of the CoFe-500 was about 51 %, which was higher 2.5 times than that of FDA-approved indocyanine green (15.1 %). Dong Wang et al. constructed SnS_2 for efficient PTT (Figure 3c).[69] Different compounds also show different photothermal conversion efficiency. For instance, the as-prepared SnS_2 exhibited helical bowl-like structure and had excellent photothermal properties and good biocompatibility, and η is as high as 57.8 %. Because of its outstanding photothermal response, it can be used as a highly efficient near-infrared photothermal agent, which can effectively inhibit and kill cancer cells. Ruiping Zhang et al. designed molecular dye SYL to carry out PTT (Figure 3d).[89] A novel small-molecule dye SYL nanoparticles (SYL NPs) was designed using an optimized DD-A-DD scaffold with 3,4-ethylenedioxythiophene, dialkylfluorene and diphenylamine as donor units. The synthesized SYL was applied to photothermal conversion, the calculated η of SYL NPs was 21.8 %, exhibiting an efficient photothermal conversion. Further *in vitro* studies, the results showed that more than 90 % of cell death was achieved. In the animal model study, the 808 nm laser irradiation area has obvious tumor ablation, and in a long-term recording process, the mouse tumor has been effectively suppressed.

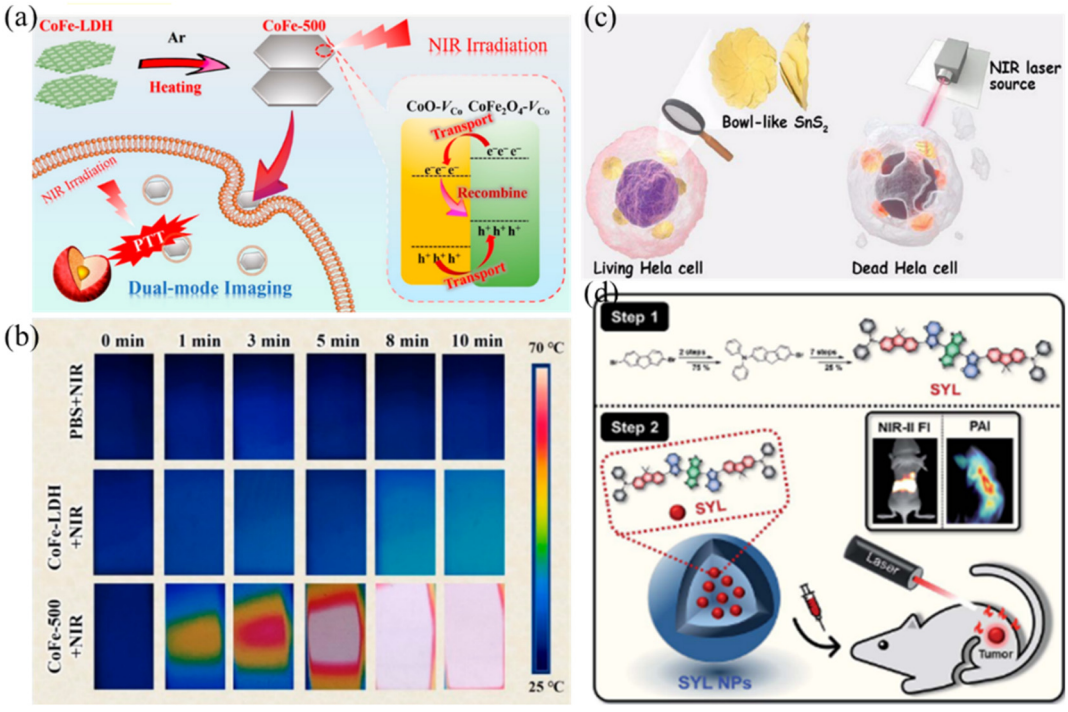

Figure 3: Photothermal therapy. (a) Schematic illustration of CoFe-LDH PTT procedure. (b) Thermal images of different samples.[67] Copyright 2020, American Chemical Society. (c) Schematical illustration of NIR-driven PTT of SnS_2.[69] Copyright 2020, Elsevier. (d) Schematic illustration of the synthesis and PTT of molecular dyes.[89] Copyright 2019, Royal Society of Chemistry.

Table 2: Summary of nanomaterials with PTT capability.

Sample	Photothermal efficiency η	Reference
Bi_2S_3/FeS_2@BSA	38.7 %	90
MnO_2	62.4 %	91
Sn_xWO_3	18.6 %	92
NBP@TiO_2	(93.3 ± 5.2)%	11
Gd:CuS@BSA	32.3 %	7
$MoS_2/Cu_{1.8}S$	32.5 %	93
Mxenes	30.6 %	8

PTT uses high heat for local tumor ablation to achieve good results, and high photothermal conversion efficiency is one of the most sought performance indicators in the study. Other nanomaterials with photothermal conversion capability are summarized in Table 2. While photothermal therapy has demonstrated significant promise in the realm of tumor treatment, it currently remains confined to the realms of fundamental and clinical research, with a notable gap separating it from widespread clinical implementation. This predicament primarily stems from the existence of several technical hurdles that necessitate resolution, including the restricted penetration depth of laser beams, the precise determination of optimal treatment temperatures, and the selection of suitable materials for photothermal conversion reagents.

4.2 Photodynamic strategy

Compared with traditional therapies, PDT has received increasing attention due to their low systemic toxicity, high selectivity and minimal invasiveness.[94] Photodynamic therapy primarily functions by activating photosensitizers, which then generate reactive oxygen species (ROS) endowed with redox activity. These ROS subsequently interact with cellular components, leading to the disruption of cellular structures. Typically, the efficacy of antitumor treatment is positively correlated with the quantity of ROS produced by the photosensitizer; that is, a greater yield of ROS tends to yield more robust antitumor outcomes. Johannes Karges et al. designed a ruthenium (II) polypyridine complex with (E, E ′)-4,4′-distyrene 2,2′-bipyridine ligands for photodynamic therapy.[15] The utilization of photosensitizers is constrained by several factors, including their inadequate water solubility, propensity for aggregation, susceptibility to photobleaching, and sluggish clearance from the body. The results show impressive photon absorption with a higher absorption amplitude than has been published to date.

Although non-toxic in the dark, these compounds are phototoxic in a variety of 2D monolayer cells, 3D multicellular tumor spheres, and are capable of eradicating multidrug-resistant tumors within mouse models under clinically relevant photon excitation. Wenxian Du et al. fabricated Ce6/MnO_x@HMSNs–PEG (CMHP) to carry out the theranostic of tumor (Figure 4a). For the first time, they proposed an intelligent "on/off" strategy co-anchored by MnO_x and Ce6 in MSNs. The multi-functional therapeutic nanoplatform CMHP exhibits a sensitive longitudinal relaxation signal to overexpressed hydrogen. At the same time, Mn^{2+} reacted with hydrogen peroxide to produce high-intensity ROS, which promoted cell death. Rongcheng Han et al. constructed AuNC@DHLA to perform two-type photonic excited PDT. The therapeutic effect of the AuNC@DHLA material was evaluated by the tumor model *in vivo*.[13] As shown in Figure 4b, compared with the control group, the treatment group with light and AuNC@DHLA material injection observed a significant tumor inhibition effect, providing that AuNC@DHLA was very effective in inhibiting xenograft tumor growth. The five mice treated with AuNC@DHLA showed a more significant reduction in tumor volume compared to the control group (Figure 4c). During the course of nanomaterials-based therapy, the issue of toxicity remains a significant concern. To evaluate the potential toxicity of the material, tissue sections were obtained from mice that had undergone treatment. The findings revealed no discernible abnormalities or pathological lesions following treatment with AuNC@DHLA, suggesting that this therapeutic approach does not elicit any notable toxic reactions (Figure 4d). PDT stands as an innovative therapeutic modality that harnesses the synergistic interaction between photosensitizers, specific wavelengths of light, and oxygen molecules to selectively eradicate diseased cells or tissues. Its underlying principle is straightforward and well-defined, offering notable advantages such as high precision and minimal collateral damage during the treatment process. As technological advancements continue to unfold and the scope of its applications expands, photodynamic therapy is poised to assume an even more prominent role in the treatment of a broader array of medical conditions in the foreseeable future.

4.3 Sonodynamic strategy

Sonodynamic therapy, a low-intensity ultrasound therapy combined with acoustic sensitizers, has emerged as a promising cancer treatment since it was developed in the late 1980s.[18] SDT is similar to the PDT, the difference is that the stimulation light source is replaced by an ultrasound device. Compared with PDT, ultrasound has stronger penetration ability and can eliminate deep tumors. Xianwei Wang et al. designed TiO_{1+x} for SDT.[66] To improve the therapeutic response to SDT, a more effective and stable acoustic sensitizer TiO_{1+x} was designed. Compared with traditional acoustic sensitized TiO_2 nanoparticles, TiO_{1+x}, due to the introduction of oxygen vacancy defects, can act as a defect trap of ultrasound-induced carrier to inhibit the carrier reflow recombination, increase the carrier utilization rate, and thus induce the generation of reactive oxygen species (ROS) more effectively, showing a stronger SDT effect (Figure 4e). To further improve the catalytic activity of traditional TiO_2, heterostructures Nb_2C/TiO_2/BSO-PVP have also been developed by Xin Guan et al. to enable efficient SDT. As shown in Figure 4f, the Nb_2C nanosheets were employed as a scaffold to house the TiO_2 acoustic sensitizer and L-butylthionine-sulfoxylamine. The findings revealed that Nb_2C/TiO_2/BSO-PVP effectively mitigates ROS consumption by impeding glutathione synthesis. Additionally, it significantly enhances the efficiency of electron-hole pair utilization and promotes the separation of electron-hole pairs within heterogeneous structures, thereby augmenting ROS production. Wenwen Yue et al. also fabricated nanosonosensitizers (HMME/R837@Lip) to perform SDT. The liposome was used as a carrier to co-encapsulate a sonar sensitizer (haematoporphyrin monomethyl ether (HMME)) and an immune adjuvant (imiquimod (R837)). As a result, the as-prepared HMME/R837@Lip enhanced SDT by combining with anti-PD-L1, and further inducing an anti-tumor response. This results not only hindered the advancement of primary tumors but also curtailed the incidence of lung metastasis. These significant advancements offer profound insights and guidance for the development of highly effective SDT nanoplatforms. In contrast to optical therapies, SDT represents an innovative approach to tumor treatment with extensive application potential. It leverages the activating effects of ultrasonic energy and sonosensitizers to dismantle tumor tissue, offering advantages such as non-invasiveness, minimal discomfort, reduced side effects, and a broad spectrum of treatment capabilities.

4.4 Radiosensitizer strategy

Radiation therapy is a form of treatment that uses ionizing radiation beams applied externally to eradicate tumors.[6] However, radiotherapy technology requires high ionizing radiation energy to deal with damaged tumor cells, and also has a killing effect on normal tissues, which may have strong side effects. In order to reduce the side effects of radiotherapy, the use of nano radiotherapy sensitizer can reduce the energy of radiotherapy beam, while increasing the production of ROS, so as to achieve good radiotherapy effect.

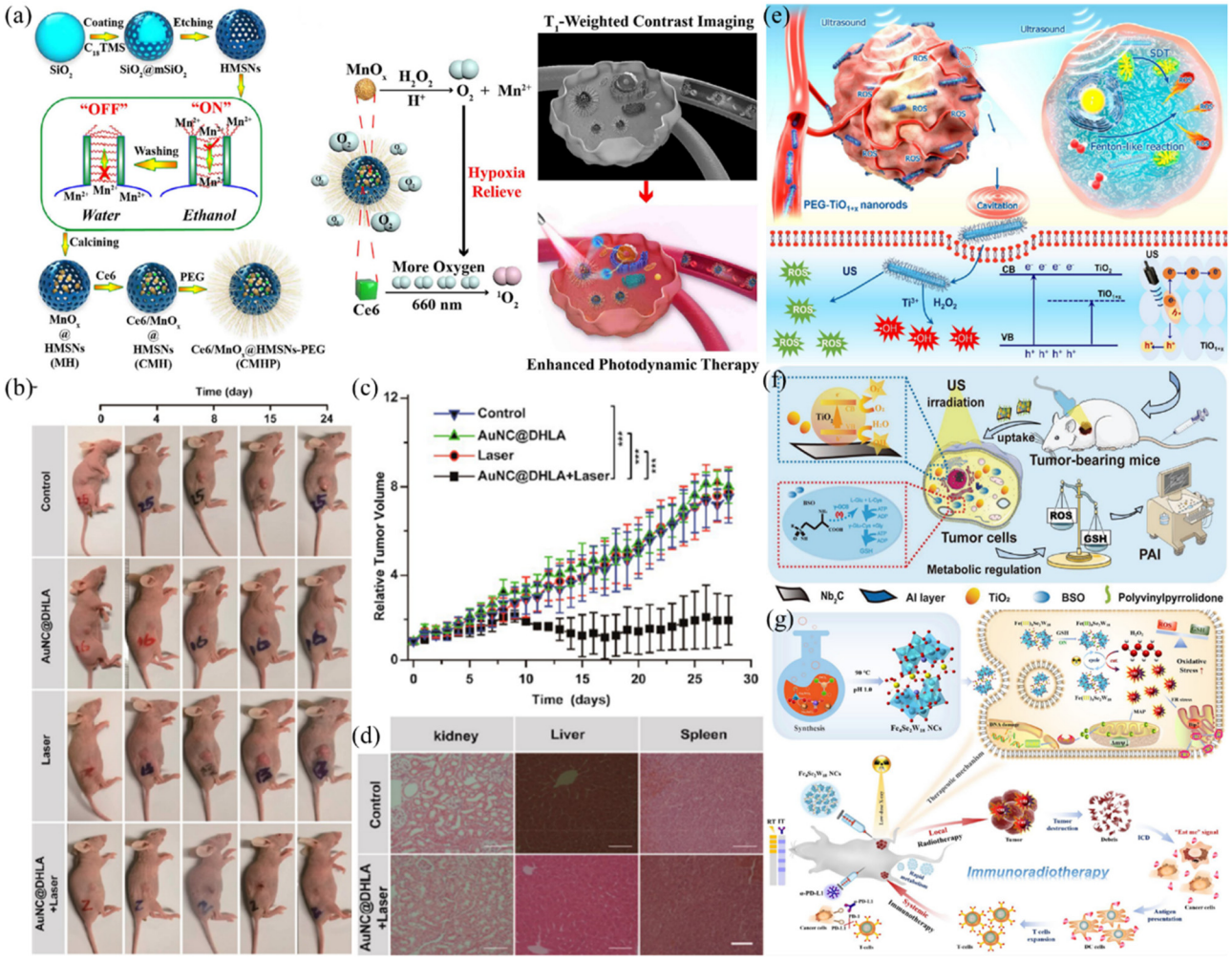

Figure 4: Antitumor therapy. (a) Illustration of preparation of CMHP and antitumor.[14] Copyright 2020, Elsevier. (b) Photographs of mice with different treatments. (c) Curves of relative tumor growth. (d) H & E staining pictures of different tissues.[13] Copyright 2019, American Chemical Society. (e) Schematic illustration of TiO_{1+x} SDT mechanism.[66] Copyright 2020, American Chemical Society. (f) SDT illustration of Nb_2C/TiO_2/BSO-PVP.[17] Copyright 2020, Wiley. (g) Schematic illustration of $Fe_4Se_2W_{18}$ RT.[95] Copyright 2021, Elsevier.

Based the purposed mentioned above, Ruyi Zhou et al. designed $Fe_4Se_2W_{18}$ nanoclusters to carry out the RT.[95] In addition to enhancing X-ray deposition to reduce dose, $Fe_4Se_2W_{18}$ NCs also exhibited catalytic activity in response to the tumor microenvironment, primarily through GSH dissipation and Fenton reaction. Under X-ray irradiation, $Fe_4Se_2W_{18}$ NCs produced a cascade of hydroxyl radicals, enhances tumor-specific oxidative stress, and not only selectively ablates local tumors, but also effectively activates anti-tumor immune responses (Figure 4g). Meanwhile, Guosheng Song et al. further summarized the application of nanosensitizers in the radiotherapy process, providing a reliable perspective for the development of more advanced nanosensitizers.[96] Radiation therapy is an important means of tumor treatment, which has wide application prospect and remarkable curative effect. However, before receiving treatment, it is necessary to fully understand its principle, treatment mode, precautions and possible side effects, and then work hard to alleviate the side effects of radiotherapy, with the advantages of nanomaterials to reduce side effects.

4.5 Gas strategy

Gas therapy is mainly the use of nanomaterials to deliver or produce cytotoxic gases under external action, such as carbon monoxide, nitric oxide, sulfur dioxide and hydrogen sulfide etc., for anti-tumor therapy. Carbon monoxide (CO) is an endogenous gas molecule that has been found to have a wide range of effects on apoptosis. Direct use of carbon monoxide is also thought to have a pro-apoptotic effect on cancer cells while reducing toxicity to normal cells.[20] CO is a

colorless, odorless gas that is known to be toxic and even deadly in high concentrations. Ying Zhu et al. carried out the GT by using the CO release under the light irradiation.[19] They designed the POBNS-PEG by introducing the intermediate band for the bismuth nanomaterials, as a sensitive producer of intracellular CO, it can reduce CO_2 to CO under red excitation (Figure 5a). In the meantime, the CO generated by POBNS-PEG has the potential to enhance the efficacy of chemotherapy while concurrently mitigating the inflammatory responses induced by PTT. When compared to alternative nanosystems, this standalone, multifunctional POBNS-PEG system exhibits distinct advantages, including a straightforward composition, streamlined production processes, and heightened biosafety. These findings serve as a pivotal reference point for the advancement of gas therapy (GT) nanomaterial systems. Within the realm of gasotransmitters, nitric oxide (NO) stands as the pioneering member, playing a critical role in both physiological and pathological processes. NO can even engage in reactions with ROS to yield highly reactive peroxynitrite ($ONOO^-$) molecules and other reactive nitrogen species (RNS). These reactive species are believed to be exceptionally potent oxidants, capable of intensifying cellular damage through the initiation of free radical-induced peroxidation reactions and augmenting the therapeutic impact of ROS on tumor tissues. Nevertheless, given the high reactivity and exceedingly brief half-life of NO (ranging from 1.5 to 6 min) in buffered solutions or plasma, the challenge persists in effectively delivering NO within biological systems and orchestrating the synchronized release of NO and ROS to generate RNS. Therefore, Jie An et al. employed the GSNO/Ce6@ZIF8@Cytomembrane to kill tumor after generating the NO.[97] Firstly, the compound GSNO, which has the activity of NO production, is linked to the surface of nanomaterials through chemical coordination, and then coated with some fluorescent materials for photo-induced ROS production, and modified by specific tumor cell membranes to improve homologous targeting ability (Figure 5b). As a result, NO released by GSNO and ROS produced by Ce6 are both triggered by US and react with each other to produce highly active $ONOO^-$ molecules and other RNS, significantly enhancing tumor clearance. This effective tumor therapy approach provides a new strategy for exploring high-performance antitumor methods.

4.6 Synergistic strategy

Collaborative therapy is a treatment mode formed by the combination of two or more treatments, which can avoid the shortcomings of insufficient combination of single treatment mode and achieve more efficient tumor treatment. This treatment mode is also the most widely used and the most popular treatment program. For instance, PTT/PDT,[70,98–104] PTT/RT,[105] PTT/PDT/chemo-therapy,[65,106] chemo-therapy/PDT,[107] chemo-PTT,[93,108–110] PTT/RT,[111] SDT/GT[97] etc. Collaborative treatment strategies offer significant advantages in achieving precise diagnosis and targeted therapy, ultimately enhancing tumor cell eradication. The localized hyperthermia generated by PTT not only directly eliminates tumor cells through thermal ablation but also improves tumor tissue oxygenation by disrupting tumor vasculature and impeding nutrient supply. This, in turn, augments the efficacy of ROS production in PDT, creating a synergistic therapeutic effect. Similarly, the integration of radiotherapy techniques with SDT can induce tumor vascular normalization, alleviate tumor hypoxia, and amplify radiotherapy outcomes. Radiotherapy is inherently more effective against oxygenated cells, yet hypoxic tumor cells in the core regions often exhibit resistance. Photothermal therapy addresses this limitation by dilating tumor blood vessels, increasing oxygen delivery, and thereby sensitizing hypoxic cells to radiotherapy-induced damage. In summary, the strategic application of collaborative treatment modalities–such as photothermal-radiotherapy combinations–demonstrates superior efficacy. By leveraging the complementary strengths of these approaches, clinicians can achieve more precise disease management and more potent anti-tumor responses, ultimately advancing patient outcomes.

5 Possible antitumor mechanisms

The tumor microenvironment is an important place for tumor occurrence, development and metastasis. Nanomaterials can play an antitumor role by regulating the tumor microenvironment. Some nanomaterials can produce cytotoxic substances, which can destroy biological macromolecules such as DNA, proteins and lipids of tumor cells, leading to tumor cell apoptosis. In addition, nanomaterials can also activate apoptosis signaling pathways of tumor cells, such as mitochondrial pathway, death receptor pathway and endoplasmic reticulum stress pathway, so as to induce apoptosis of tumor cells (Figure 6).[112] Nanomaterials can also activate the immune system to exert anti-tumor effects. By designing immunologically stimulating nanomaterials, immune cells in the tumor microenvironment, such as macrophages, dendritic cells and natural killer cells (NK cells), can be activated to enhance their ability to recognize and attack

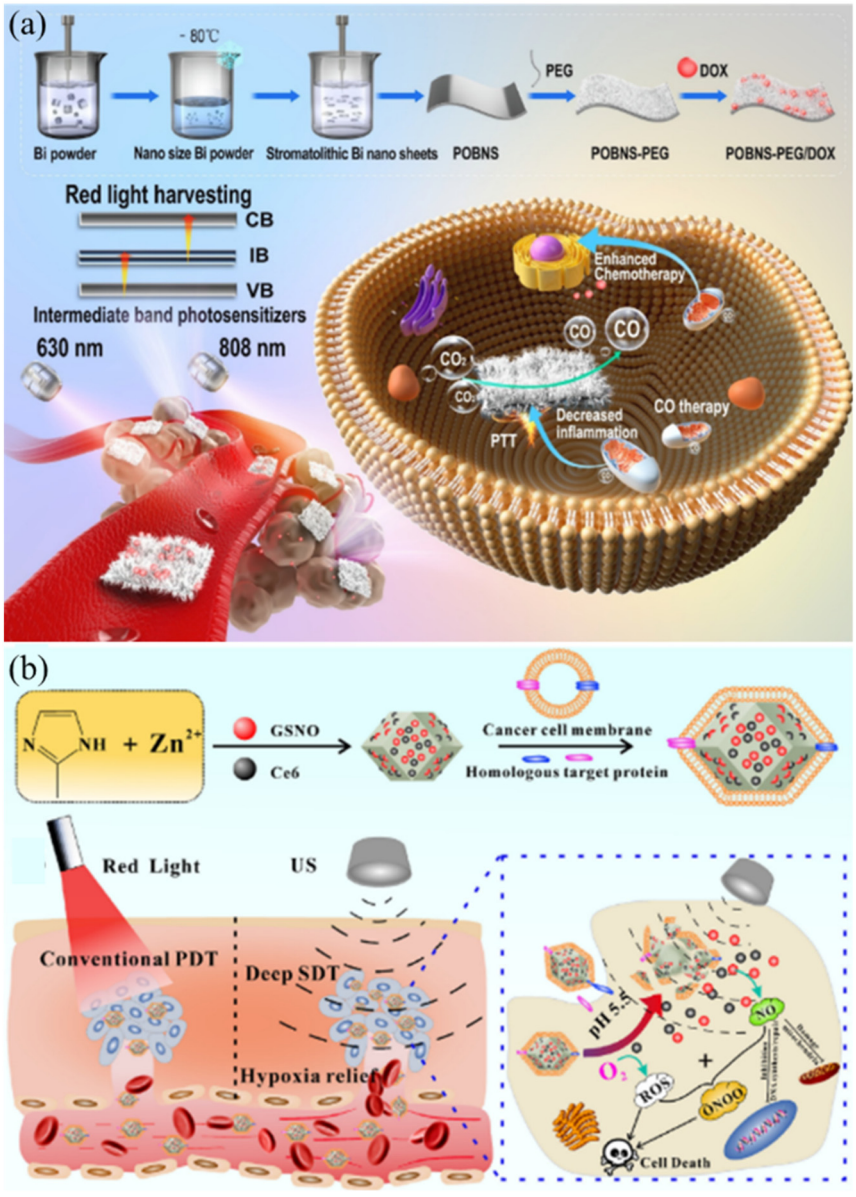

Figure 5: Schematic diagram of the synthesis and treatment of nanomaterials. (a) Schematic illustration of POBNS-PEG GT system.[19] Copyright 2022, Elsevier. (b) Schematic illustration of preparation and GT application of GSNO/Ce6@ZIF8@Cytomembrane.[97] Copyright 2020, Elsevier.

tumor cells. In addition, nanomaterials can also act as immune adjuvants to improve the immune effect of vaccines, thereby inducing a stronger anti-tumor immune response. Nanomaterials can also be combined with other therapies to play a synergistic anti-tumor role. For example, nanomaterials can be used as sensitizers for phototherapy, hyperthermia or radiotherapy, improving the efficacy of these treatments. In addition, nanomaterials can also be combined with chemotherapy drugs, targeted drugs or immunotherapy drugs, etc., to form a multi-modal treatment strategy, so as to more comprehensively inhibit tumor growth and metastasis.

6 Imaging CAs applications

6.1 X-ray CT CAs

CT imaging is a widely used disease diagnosis method in clinical practice, and the location of the disease and related anatomical information can be clearly observed through 3D imaging mode. Although this method can achieve non-destructive and rapid disease diagnosis, due to its strong X-ray absorption imaging ability for high-density substances, it cannot achieve good imaging function for soft tissues with light density mass, especially for the diagnosis of

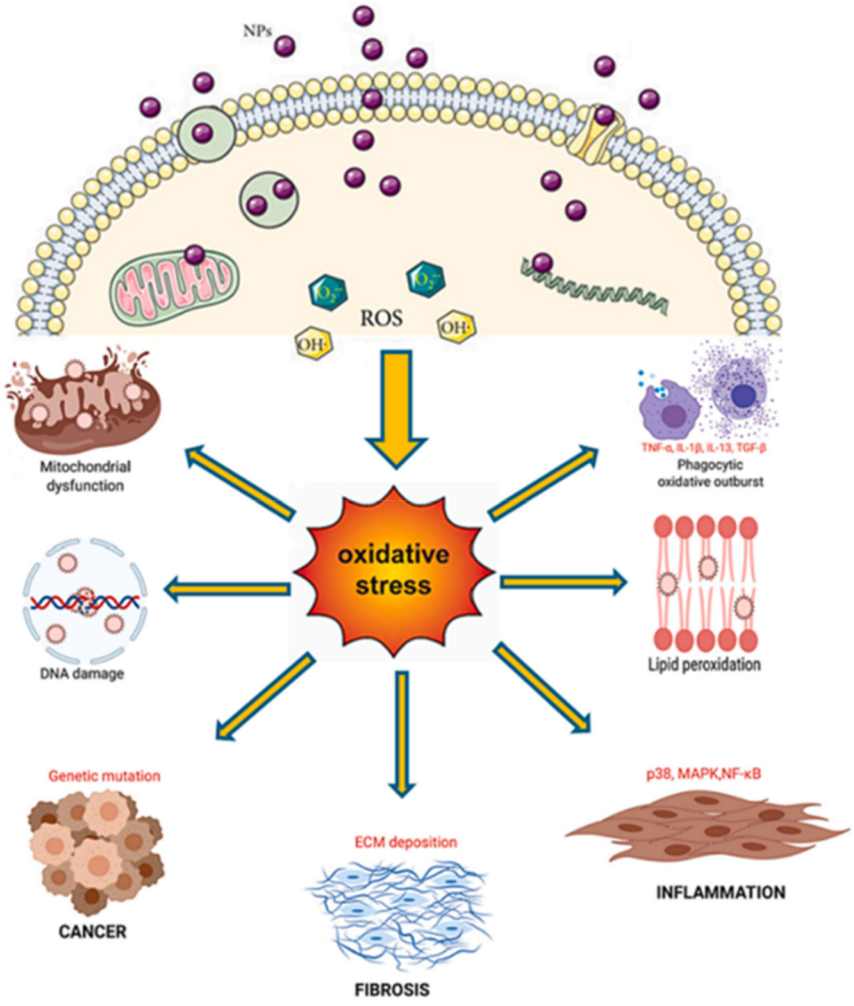

Figure 6: Schematic illustration of possible antitumor mechanism.[112] Copyright 2023, Elsevier.

diseases such as blood vessels. Therefore, contrast agents are needed to enhance the function of contrast imaging and achieve accurate diagnosis of diseases. At present, small molecule compounds containing iodine, such as iodohexyl alcohol and iodoxanol, are used as contrast agents in clinical practice, which can achieve good imaging function. However, due to the rapid metabolism of solution with short circulation time of small molecules, it is not conducive to the grasp of imaging time, usually requiring large amounts of injection, and easy to cause renal toxicity. Therefore, in order to solve the disadvantages of clinical contrast agents, nanomaterials with appropriate scale can extend the cycle time, and large specific surface area can achieve modification and reduce cytotoxicity. Using nanomaterials as CT contrast agents points out a new direction for the study of novel CAs. Pratap C. Naha et al. designed CeO_2 as CAs to perform CT imaging.[59] As shown in Figure 7a, compared to clinical contrast agents, CeO_2 nanomaterials can also achieve a good enhanced imaging capability, showing a clear gastrointestinal profile. It was noteworthy that the CeO_2 had a longer retention time in the body after injection, which can be more convenient to observe the lesion clearly, without strictly controlling the time and large dose of injection, reducing the side effects of the contrast agent on the body. Maryam Hosseini et al. used SBBHs to carry out the CT imaging.[60] After intravenous injection, the results can show enhanced imaging effect. Clinical contrast agents can be metabolized by the kidney due to the small molecule properties described above, while SBBHs is basically absorbed and metabolized by the liver. Similarly, small molecule drugs have a relatively short cycle time and are quickly metabolized from the body, while nanoparticles have a longer cycle time and are able to accumulate over a period of time, a result consistent with most studies (Figure 7b). Importantly, the use of contrast media can play a more accurate function in the diagnosis of vascular diseases (Figure 7c), and provide a reference for making up for the deficiency of clinical

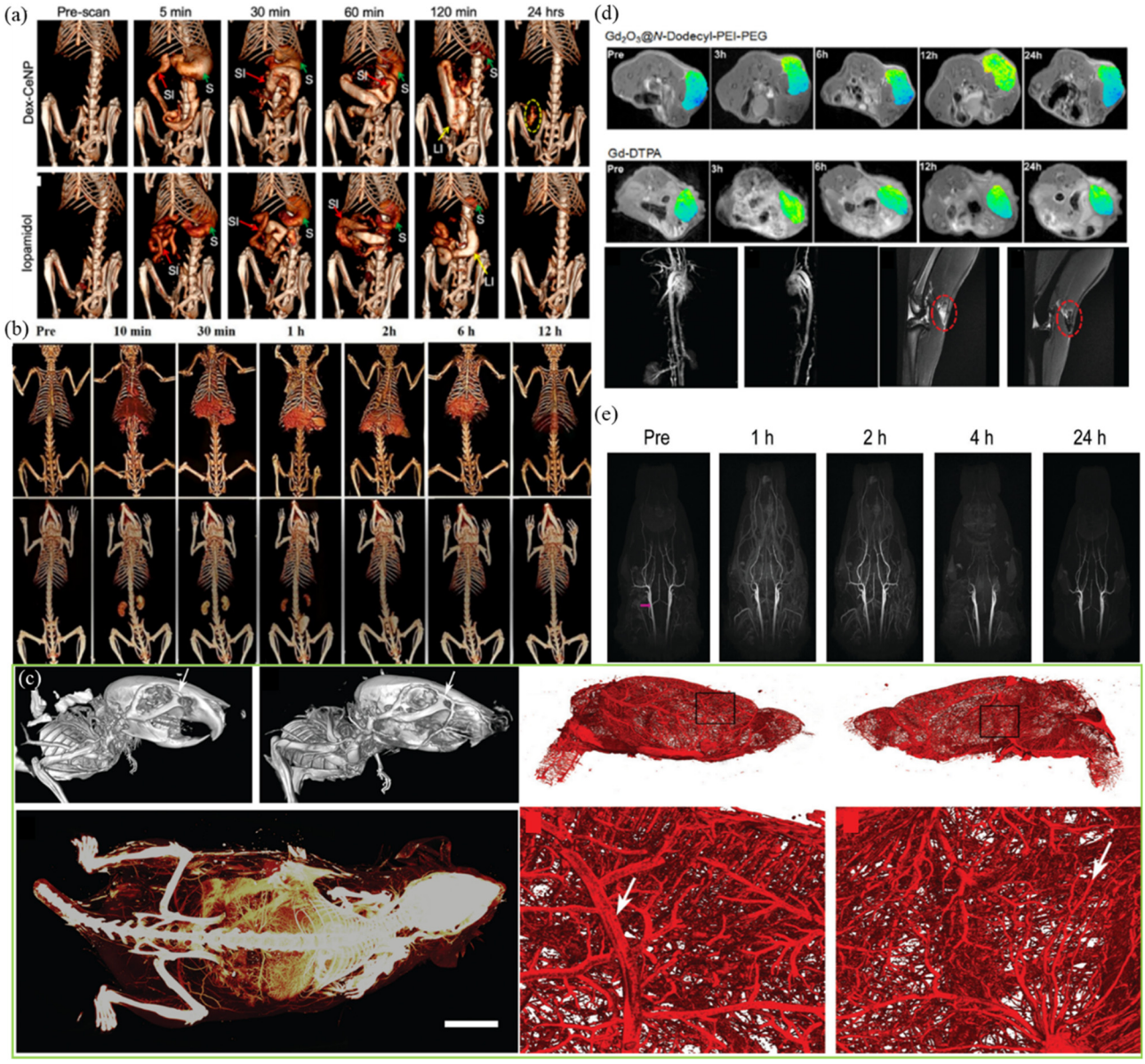

Figure 7: Nanomaterials for CT imaging. (a) CT imaging of gastrointestinal tract *in vivo*.[59] Copyright 2020, American Chemical Society. (b) CT images of mice before and after injection of SBBHs CAs.[60] Copyright 2020, American Chemical Society. (c) X-ray imaging of vascular system.[113] Copyright2020, Royal Society of Chemistry. (d) T1-weighted MRI images of Gd_2O_3 nanoparticles.[36] Copyright 2020, Elsevier. (e) MRI angiography of rat brain.[114] Copyright 2019, Royal Society of Chemistry.

angiography. CT contrast agent can optimize the tissue structure information, so that it can be better diagnosed.

6.2 MRI CAs

Magnetic resonance imaging has great advantages in detecting soft tissue, which relies on proton relaxation ability in water to obtain image information. MRI is divided into two imaging modes, including T1 and T2, generally in order to clearly obtain more useful tissue information, usually use contrast media. In most cases, Gd-based contrast agents are used, which can lead to renal fibrosis and renal impairment due to the leaching of free Gd^{3+} ions from gadolinium complexes. In addition, after repeated exposure to Gd^{3+}, gadolinium can accumulate in a patient's bones and even brain tissue and remain in these organs for years.[31,33] In order to solve these problems, the use of nanomaterials for imaging can effectively reduce toxicity and enhance imaging time. Wen Cai et al. constructed Gd_2O_3 nanoplates for performing T1-weighted MRI.[36] The as-prepared Gd_2O_3 exhibited an average size of 95 nm, and the R1 value was

14.13 $mM^{-1} s^{-1}$, achieving a stronger MRI capability. As shown in Figure 7d, a false-color T1-weighted MR Images before and after injection of Gd_2O_3 clusters and commercial Gd-DTPA (control group) with SCC-7 xenograft tumor were recorded on a 9.4T MRI apparatus. It can be seen that the contrast of tumor areas was significantly enhanced after injection of Gd_2O_3 cluster. In addition, T2-weighted MR imaging also exhibited good tissue information. The safety concerns of Gd-based drugs have prompted research into alternative materials, and recently, superparamagnetic based nanomaterials have been reported to achieve T2 enhanced MR Effects. Lateral (T2) contrast is enhanced by inducing local magnetic field inhomogeneity, which degrades nearby water particles and shortens T2* and T2 relaxation.[115] Chongchong Miao et al. constructed dual-functional Fe_2O_3 CAs for T1/T2 MR imaging.[35] The as-prepared Fe_2O_3 CAs achieved a satisfactory R1 = 10.7 mM^{-1} s-1 and R2 = 38 $mM^{-1} s^{-1}$, indicating an effective T1/T2-weighted imaging ability. The T1-weighted contrast effect of Fe_2O_3 CAs on in angiography was evaluated *in vivo*. The results showed that the injection dose of 150 mmol Fe/kg can clearly observe the blood vessel images, even the small blood vessels in the renal artery and the branches around the pulmonary artery could be well observed, which fully demonstrated the good angiographic ability of Fe_2O_3 CAs. Moreover, T2-weighted MRI images of rabbit popliteal lymph nodes were obtained. The results showed that the lymph node signal intensity decreased significantly, suggesting the great potential of Fe_2O_3 CAs as a bifunctional contrast agent. Importantly, the change of morphological structure can significantly affect the relaxation ability of the material, and thus affect the contrast ability in magnetic resonance imaging.[116] Yao Cai et al. prepared good biocompatible iron oxide nanoparticles to achieve T2 angiographic imaging, providing good guidance for the diagnosis of vascular diseases (Figure 7e). Other MRI CAs are studied and shown in Table 3. Although the re-performance of these nano-contrast agents is better than that of clinical small molecule contrast agents, their biosafety is very important, and more attention should be paid to the study of biosafety in the subsequent clinical pre-conversion research.

Table 3: Classification of MRI CAs.

Sample	Imaging mode	Reference
Fe_2O_3/MnO_2	T1/T2	62
Cu–Fe_2O_3	T1	34
M–HFn	T1	114
γ–Fe_2O_3	T1	117
Ba_2GdF_7	T1	53,118
Fe_2O_3	T2	119
$NaGdF_4$	T1	120

6.3 Photoacoustic imaging CAs

Photoacoustic imaging operates on the fundamental principle of the photoacoustic effect. Upon exposure of biological tissue to a pulsed laser, light-absorbing entities within the tissue absorb the incident light energy and convert it into heat, leading to localized temperature elevation and rapid thermoelastic expansion. When specific thermal and pressure thresholds are attained, this transient elastic thermal expansion of the tissue generates pressure waves, commonly referred to as ultrasonic waves or photoacoustic signals. These photoacoustic signals encode information pertaining to the optical absorption properties of the tissue. These signals are received by the ultrasonic detector located on the surface of the tissue, and after appropriate signal processing and image reconstruction algorithms, the optical absorption distribution of the tissue can be reconstructed.[105] Typically, to acquire superior image information, photoacoustic contrast agents are employed to augment the quality of image signals. When utilizing photoacoustic contrast agents, the pivotal factor to be considered for achieving optimal imaging outcomes is the photothermal conversion efficiency, as a high thermal efficiency facilitates the generation of enhanced signal output. Chengyuan Hong et al. employed defective BiOCl to carry out a satisfactory PA imaging.[121] In this study, the PA signal was enhanced with imaging time, and the position signal reaching the target was clearly observed, achieving a good diagnosis of tumor disease (Figure 8a). At the same time, it also shows that good thermal efficiency achieves good photoacoustic signal transmission. Similarly, Yuemei Wang et al. constructed 2D bismuthene as PA CAs for high-performance diagnosis. The photoacoustic signal was significantly improved before and after the use of contrast agent.[98] Generally speaking, photoacoustic imaging presents fewer side effects and causes less damage compared to X-ray imaging. Furthermore, photoacoustic imaging offers a more user-friendly approach, thereby facilitating precise diagnosis and effective treatment of tumors.

6.4 Fluorescence imaging CAs

Fluorescence is produced by the interaction of photons and molecules. Under normal conditions, most molecules are in the lowest vibration level of the ground state, when excited by light energy, electrical energy, chemical energy and other

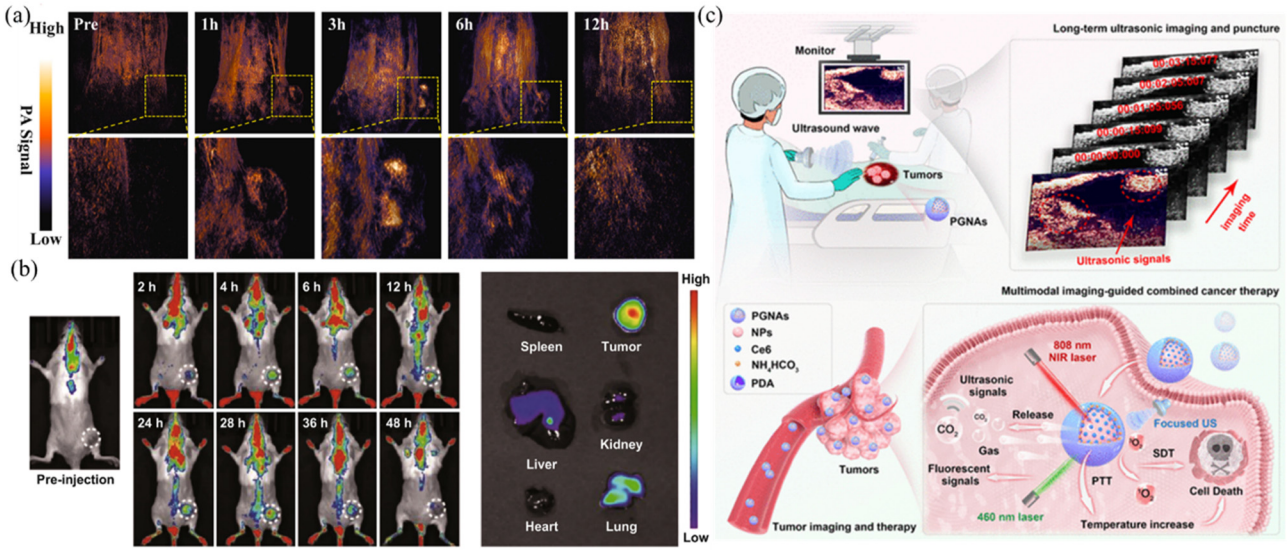

Figure 8: Different nano-diagnostic models. (a) PA imaging of defective BiOCl as CAs.[121] Copyright 2025, Elsevier. (b) Fluorescence imaging of mice after injection of nanoparticles with Ce6 loading.[94] Copyright 2020, Springer Nature. (c) Schematic illustration of ultrasonic imaging-guided cancer treatment.[122] Copyright 2024, American Chemical Society.

energy, the electrons around the nucleus will transition from the ground state level to the higher energy excited state (the first or second excited state). The excited electrons are in a high energy state and unstable, and will release energy back to the ground state in two ways: a radiative transition in the form of photon release of energy (including fluorescence and phosphorescence processes), and a non-radiative transition in the form of energy release such as heat. Typically, upon excitation, electrons outside the nucleus transition from the ground state to an excited state. Subsequently, they rapidly descend to the lowest vibrational level via a non-radiative transition. From this level, they return to the ground state, releasing energy in the form of photon radiation. This emitted light is termed fluorescence. The theoretical underpinning of fluorescence imaging lies in the linear correlation between the intensity of the fluorescence signal emitted by the excited fluorescent substance and the quantity of fluorescein present within a specific range. When the fluorescence probe is excited by a specific wavelength of light, it will emit a specific wavelength of fluorescence, and these fluorescence signals can be captured and recorded by the fluorescence imaging system. Therefore, in order to achieve good fluorescence imaging, the contrast agent needs to have good light absorption capacity and luminous efficiency. Most of the usual fluorescent contrast agents are fluorescent dyes. Nan Yang et al. employed the Ce6 for fluorescence imaging (Figure 8b).[94] In addition to fluorescent dyes, studies have found that ultra-small quantum dots can achieve fluorescent luminescence, so they are used as luminous imaging.[123] These studies not only enrich the diagnostic applications of nanomaterials in cancer therapy, but also provide guidance for the design of other nanosystems for cancer therapy. Although fluorescence imaging is relatively safe, the tissue penetration depth of its luminous efficiency and wavelength still limits its wide application.

6.5 Ultrasonic imaging CAs

Ultrasonic imaging represents a fusion of acoustics, medicine, optics, and electronics. This technology employs ultrasonic sound beams to scan the human body, and by receiving and processing the reflected signals, it generates images of internal organs. Ultrasonic imaging technology is constantly evolving, with advantages such as safety and radiation-free.[124] The use of ultrasonic contrast agents can enhance the quality of the images to obtain more information. Binbin Chu et al. innovatively designed a nanomaterial containing ammonium bicarbonate to achieve ultrasound enhanced imaging.[122] Ammonium bicarbonate exists unstable in acidic environment, releases carbon dioxide by forming salt substances, and thus achieves the function of enhancing ultrasonic imaging. The release of carbon dioxide under laser irradiation can enhance the capture of ultrasonic signals and provide methodological support for tumor diagnosis (Figure 8c). In addition to carbon dioxide as a contrast signal enhancing gas, nitrogen, hydrogen and oxygen can also be used as CAs.[124] In summary, the effective encapsulation of gases using nanomaterials as carriers is

both the key and the foundation for achieving high-quality ultrasonic imaging.

6.6 Other imaging CAs

In addition to the aforementioned imaging techniques, which have long served as cornerstones in medical diagnostics, several emerging and specialized modalities are increasingly being leveraged to enhance diagnostic precision and therapeutic decision-making. Positron Emission Tomography (PET) using isotopes such as PET,[125] for instance, offers unparalleled insights into metabolic and functional processes at the molecular level, enabling clinicians to detect early-stage diseases, monitor treatment responses, and identify recurrence with heightened sensitivity. This non-invasive imaging approach capitalizes on the biological behavior of radiotracers, which accumulate preferentially in areas of increased metabolic activity–a hallmark of many pathologies, including cancers and inflammatory disorders. Optical coherence tomography (OCT),[63,126] another cornerstone of high-resolution imaging, employs near-infrared light to generate cross-sectional images of biological tissues at micrometer-scale resolutions. Where its ability to resolve subsurface structures in real time is invaluable. OCT's capacity to differentiate between tissue layers, detect microstructural abnormalities, and guide minimally invasive interventions underscores its versatility in both diagnostic and therapeutic contexts. Photoluminescence (PL),[127] including fluorescence and phosphorescence techniques, exploits the emission of light from molecules excited by external energy sources. This modality is particularly promising in molecular imaging, where fluorophore-labeled probes can target specific biomarkers, cells, or tissues, enabling visualization of biological processes at the cellular and subcellular levels. Magnetic particle imaging (MPI)[128] is a relatively novel technique, and leverages the magnetic properties of superparamagnetic iron oxide nanoparticles (SPIONs) to generate high-resolution images of their distribution within the body. Unlike traditional MRI, MPI offers superior sensitivity to trace amounts of magnetic nanoparticles, making it ideal for tracking cell trafficking, monitoring drug delivery, and imaging vascular processes. Its quantitative capabilities and lack of ionizing radiation further position MPI as a safe and effective tool for longitudinal studies and personalized medicine. The integration of these imaging modalities–each with its unique strengths and complementary applications–forms the backbone of multimodal imaging strategies. By combining anatomical, functional, and molecular information, clinicians can achieve a more comprehensive understanding of disease pathogenesis, progression, and response to therapy. This synergistic approach not only enhances diagnostic accuracy but also facilitates tailored treatment plans, reduces unnecessary interventions, and improves patient outcomes. As imaging technologies continue to evolve, their fusion will undoubtedly play a pivotal role in the future of precision medicine.

7 Modification strategies for enhanced therapeutic applications

In the pursuit of achieving precise optical diagnosis and treatment, the photothermal conversion efficiency and catalytic performance of nanoscale diagnostic and therapeutic agents stand as pivotal determinants within photothermal and photodynamic anti-tumor paradigms. These attributes directly govern the generation of thermal energy and the production of reactive species, thereby exerting a substantial influence on anti-tumor efficacy. Consequently, enhancing light absorption and utilization emerges as a prerequisite for attaining robust photothermal/photodynamic anti-tumor capabilities. An ideal nanoscale diagnostic agent should exhibit superior light absorption and utilization efficiency, coupled with high photothermal conversion efficiency and efficient photoelectron migration capabilities. Regrettably, many simple nanotherapeutics encounter obstacles such as limited light absorption spectra, suboptimal light energy conversion rates, and photoelectron recombination, all of which culminate in diminished optical activity and subpar diagnostic and therapeutic outcomes. Addressing these challenges to effectively augment optical efficiency and activity remains a formidable endeavor. Below, several strategic recommendations are proposed to mitigate these issues.

7.1 Defect construction and heterojunction

The introduction of defects can achieve extended light absorption capacity and enhance the optical PDT effect by boosting the separation of electron induced by defective electron trap.[129,130] At the same time, the existence of defects of different concentrations can trigger electron relaxation,

reduce the migration distance of electrons, and cause the phenomenon of photothermal conversion.[51,131] Chen Dai et al. designed defective engineering BiOCl for carrying out PTT.[71] In this work, they reasonably regulated the oxygen-defects for enhancing the photothermal conversion efficiency by controlling the ultraviolet irradiation time. As shown in Figure 9a, the temperature of BiOCl with different defect concentrations was dramatically increased with the ultraviolet irradiation time. The temperature of BiOCl can achieve 65 °C after 12 h ultraviolet irradiation treatment. Further, this work provided a valuable insight for exploring highly efficient PTT candidates by regulating the defective concentrations. Additionally, oxygen defects can be contained in some oxygen, and oxygen molecules can be released in the oxygen-poor environment to improve tumor hypoxia, and then exogenous and endogenous oxygen molecules are effectively converted into superoxide anions to enhance the therapeutic effect.[64] Heterogeneous materials, serving as a crucial medium for ROS generation, leverage the interface effect between disparate materials to effectively integrate light-absorbing materials and catalysts, thereby forming heterogeneous structures. These structures markedly enhance the efficiency and selectivity of photocatalytic reactions for ROS production, consequently facilitating potent PDT effects. Moreover, heterogeneous architectures also play a pivotal role in photothermal catalysis. Through reasonable material selection and structural design, efficient light energy absorption and heat energy conversion can be achieved, so as to improve the efficiency of photothermal catalysis.[132,133] It facilitates the coupling of efficient light absorption with low thermal conductivity, thereby elevating the irradiation temperature of photothermal materials. This enhancement aids in driving a greater number of catalytic reactions, ultimately improving the efficiency of photothermal catalysis. Concurrently, by optimizing the design and synthesis of heterogeneous structures, higher photothermal conversion efficiency can be achieved, allowing for the conversion of more light energy into heat energy, which can be harnessed to drive photothermal therapy PTT. The heterojunction can construct the insert electric field to adjust the photoinduced carrier migration efficiency, so that more carriers can be converted into ROS to enhance the PDT effect (Figure 9b). Meanwhile, the electrons stimulated by light irradiation can migrate across the interfaces of nanomaterials, effectively impeding the backflow and recombination of photogenerated carriers, thereby enhancing the PDT efficacy. Consequently, the judicious design of heterogeneous materials can orchestrate a synergistic effect of

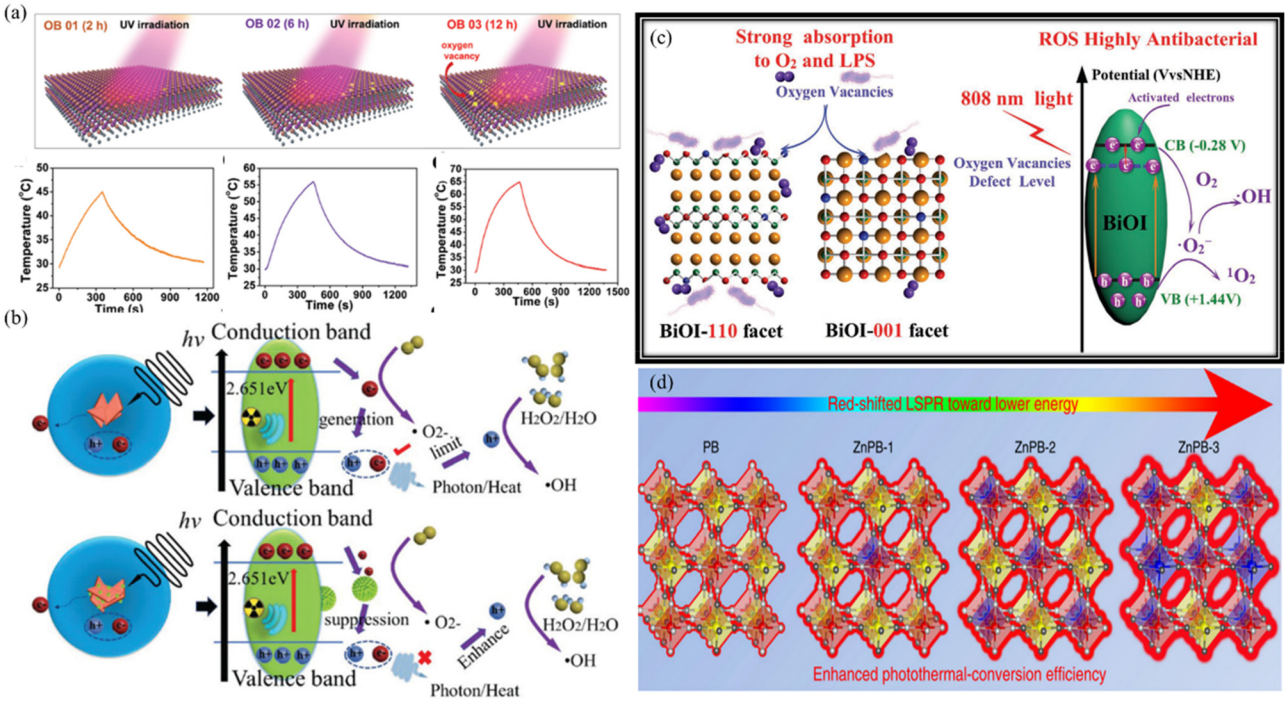

Figure 9: Schematic diagram of strategies for enhancing the performance of nano-therapeutic agents. (a) Photothermal conversion of BiOCl with different concentrations of oxygen defects.[71] Copyright 2020, Royal Society of Chemistry. (b) Schematic illustration of the enhancement of PDT.[134] Copyright 2021, Royal Society of Chemistry. (c) Schematic of a possible photocatalytic antimicrobial mechanism with different face exposures.[135] Copyright 2020, Wiley-VCH. (d) The enhancement of photothermal conversion by ion doping.[136] Copyright 2019, Springer Nature.

multiple therapeutic modalities, ultimately yielding more satisfactory treatment outcomes.

7.2 Morphological effect and facet exposure

There is a close relationship between morphological effect and light absorption capacity and drug carrying capacity. For example, ultra-thin structures have the advantages of large specific surface area, electron limitation, and more atoms exposed on the surface, allowing for efficient construction of active sites and surface structural modifications that exhibit different physicochemical properties.[137–139] The ultra-thin structure allows a short migration distance for the rapid diffusion of photoexcited carriers from the body to the surface, thereby inhibiting electron-hole pair recombination.[140] Unfortunately, despite the widespread application of nanomaterials with diverse morphologies in photocatalytic applications, nanosystems with varying morphological structures remain understudied in the context of tumor therapy. Consequently, it is imperative to delve into the morphological antitumor effects. By finely tuning the facet exposure of nanomaterials, it is possible to efficiently achieve satisfactory photodynamic therapy (PDT) outcomes, while favorable surface exposure can also bolster photothermal conversion efficiency.[141] The structural attributes of distinct crystal faces vary significantly, encompassing aspects such as atomic arrangement, surface density, and the quantity of active sites, all of which collectively dictate the catalytic activity of a catalyst for various reactions. Typically, catalysts with fewer atoms on their crystal surfaces (indicating lower surface density) exhibit a greater number of active sites, thereby resulting in heightened reaction activity. Furthermore, different crystal faces may exert an influence on the PDT activity of nanomaterials, rendering the investigation of PDT nanomaterials with varying crystal face exposures of paramount importance. Li et al. demonstrated that exposure on the surface of anisotropic crystals allows the directed transfer of photoexcited electrons (e^-) and holes (h^+), enabling space charge separation and thus enhancing photocatalytic activity.[142] Jingyu Sun et al. designed BiOI with different exposed facets, such as {001} (BI-001) and {110} (BI-110) for high-performance antibacterial activity. The BI-110 can absorb more oxygen and bacteria, resulting in the production of large singlet oxygen for bacterial elimination (Figure 9c). This research has substantiated the optimization capabilities of crystal facet engineering in enhancing photocatalytic activity, thereby playing a pivotal role in augmenting photocatalytic performance. These findings further suggest that substantial efforts can be directed towards facet engineering to explore efficient avenues for PDT.

7.3 Ion doping

Ion doping can introduce intermediate impurity levels between the band gaps, reduce the electron transition distance, and increase the light absorption capacity.[143] Simultaneously, ion doping has the potential to induce lattice distortion and generate defects through the introduction of impurity ions, phenomena that can significantly influence optical properties and may stimulate photothermal conversion processes. Jun Li et al. verified the Zn-doping that can decrease the bandgap of nanomaterials,[136] further enhancing the light absorption. Of note, the effective dopant can generate the enhancement of photothermal conversion (Figure 9d). The potential mechanism underlying photothermal conversion can be attributed to the enhanced electron relaxation capacity facilitated by a reduction in the bandgap. This phenomenon bears similarities to the photothermal conversion triggered by defective engineering. Collectively, the judicious application of effective ion doping serves as a source of inspiration for augmenting the synergistic effects of PTT and PDT.

8 Conclusion and outlook

In conclusion, this review offers a comprehensive summation of the recent advancements in the diagnostic and therapeutic realms of nanomaterials. It emphasizes the classification and in-depth application of nanomaterials, thereby establishing a solid foundation for precise diagnosis and treatment. Significantly, the discourse on augmenting the therapeutic efficacy of nanomaterials acts as a cornerstone guide for the development of highly effective nanoscale theranostic agents. Although nanobiomedical materials exhibit promising clinical potential, their progression is hindered by several factors, thereby impeding their rapid clinical translation and application. To facilitate the rapid evolution and clinical integration of nano diagnostics, several critical issues demand attention:

(I) While numerous studies highlight the promising clinical prospects of nanomaterials, there remains a dearth of comprehensive research on their biological toxicity, particularly regarding metabolic implications.

(II) Nanomaterials retain high biological activity for a finite duration post-preparation, but prolonged retention may lead to particle aggregation or deactivation, a phenomenon worthy of consideration.

(III) The tumor microenvironment encompasses numerous factors that can influence the therapeutic efficacy of solid tumors. Adjusting various parameters within this

environment through nanomaterials, such as alleviating tumor hypoxia, reducing tumor pH, and normalizing tumor blood vessels, requires ongoing research to ultimately achieve effective anti-tumor outcomes.

(IV) In addition to magnetic fields and light, preclinical exploration should also encompass microwaves, radio frequencies, and high-intensity focused ultrasound for achieving deep tumor therapy.

(V) Efforts should be intensified to develop nanoparticles featuring suitable surface modifications and optimized tumor targeting and retention capabilities, thereby further enhancing tumor specificity and mitigating immune system damage.

Research ethics: Not applicable.

Informed consent: Not applicable.

Author contributions: The authors have accepted responsibility for the entire content of this manuscript and approved its submission.

Use of Large Language Models, AI and Machine Learning Tools: None declared.

Conflict of interest: All other authors state no conflict of interest.

Research funding: This work was supported financially by the Guizhou University Talent Program (Grant No. X2023158, X2024013), The Youth Talent Growth Project of Guizhou Provincial Department of Education (Grant No. QJJ2024026), The Youth guidance of Guizhou Provincial Basic Research Program (Grant No. QKHJC2024Y096), the Natural Science Foundation of Guizhou Province (Grant No. ZK2024-087) and Industry and Education Combination Innovation Platform of Intelligent Manufacturing and Graduate Joint Training Base at Guizhou University (No: 2020-520000-83-01-324061).

Data availability: Not applicable.

References

1. Shahbazi, M. A.; Faghfouri, L.; Ferreira, M. P. A.; Figueiredo, P.; Maleki, H.; Sefat, F.; Hirvonen, J.; Santos, H. A. The Versatile Biomedical Applications of Bismuth-Based Nanoparticles and Composites: Therapeutic, Diagnostic, Biosensing, and Regenerative Properties. *Chem. Soc. Rev.* **2020**, *49* (4), 1253–1321.
2. Liu, Y.; Ai, K.; Liu, J.; Deng, M.; He, Y.; Lu, L. Dopamine-melanin Colloidal Nanospheres: an Efficient Near-Infrared Photothermal Therapeutic Agent for In Vivo Cancer Therapy. *Adv. Mater.* **2013**, *25* (9), 1353–1359.
3. Liu, Y.; Bhattarai, P.; Dai, Z.; Chen, X. Photothermal Therapy and Photoacoustic Imaging via Nanotheranostics in Fighting Cancer. *Chem. Soc. Rev.* **2019**, *48* (7), 2053–2108.
4. Liu, S.; Pan, X.; Liu, H. Two-Dimensional Nanomaterials for Photothermal Therapy. *Angew Chem. Int. Ed. Engl.* **2020**, *59* (15), 5890–5900.
5. Dong, C.; Feng, W.; Xu, W.; Yu, L.; Xiang, H.; Chen, Y.; Zhou, J. The Coppery Age: Copper (Cu)-Involved Nanotheranostics. *Adv. Sci.* **2020**, *7* (21), 2001549.
6. Zhang, C.; Yan, L.; Gu, Z.; Zhao, Y. Strategies Based on Metal-Based Nanoparticles for Hypoxic-Tumor Radiotherapy. *Chem. Sci.* **2019**, *10* (29), 6932–6943.
7. Yang, W.; Guo, W.; Le, W.; Lv, G.; Zhang, F.; Shi, L.; Wang, X.; Wang, J.; Wang, S.; Chang, J.; Zhang, B. Albumin-Bioinspired Gd:CuS Nanotheranostic Agent for In Vivo Photoacoustic/Magnetic Resonance Imaging-Guided Tumor-Targeted Photothermal Therapy. *ACS Nano* **2016**, *10* (11), 10245–10257.
8. Lin, H.; Wang, X.; Yu, L.; Chen, Y.; Shi, J. Two-Dimensional Ultrathin MXene Ceramic Nanosheets for Photothermal Conversion. *Nano Lett.* **2017**, *17* (1), 384–391.
9. Yang, Y.; Zhu, W.; Dong, Z.; Chao, Y.; Xu, L.; Chen, M.; Liu, Z. 1D Coordination Polymer Nanofibers for Low-Temperature Photothermal Therapy. *Adv. Mater.* **2017**, *29* (40), 1703588.
10. Song, L.; Dong, X.; Zhu, S.; Zhang, C.; Yin, W.; Zhang, X.; Liu, X.; Gu, Z. Bi2 S3 -Tween 20 Nanodots Loading PI3K Inhibitor, LY294002, for Mild Photothermal Therapy of LoVo Cells In Vitro and In Vivo. *Adv. Healthcare Mater.* **2018**, *7* (22), e1800830.
11. Chen, J.-L.; Zhang, H.; Huang, X.-Q.; Wan, H.-Y.; Li, J.; Fan, X.-X.; Luo, K. Q.; Wang, J.; Zhu, X.-M.; Wang, J. Antiangiogenesis-Combined Photothermal Therapy in the Second Near-Infrared Window at Laser Powers below the Skin Tolerance Threshold. *Nano-Micro Lett.* **2019**, *11* (04), 630–649.
12. Chen, Q.; Hu, Q.; Dukhovlinova, E.; Chen, G.; Ahn, S.; Wang, C.; Ogunnaike, E. A.; Ligler, F. S.; Dotti, G.; Gu, Z. Photothermal Therapy Promotes Tumor Infiltration and Antitumor Activity of CAR T Cells. *Adv. Mater.* **2019**, *31* (23), e1900192.
13. Han, R.; Zhao, M.; Wang, Z.; Liu, H.; Zhu, S.; Huang, L.; Wang, Y.; Wang, L.; Hong, Y.; Sha, Y.; Jiang, Y. Super-efficient In Vivo Two-Photon Photodynamic Therapy with a Gold Nanocluster as a Type I Photosensitizer. *ACS Nano* **2019**, *14*, 9532–9544.
14. Du, W.; Liu, T.; Xue, F.; Chen, Y.; Chen, Q.; Luo, Y.; Cai, X.; Ma, M.; Chen, H. Confined Nanoparticles Growth within Hollow Mesoporous Nanoreactors for Highly Efficient MRI-Guided Photodynamic Therapy. *Chem. Eng. J.* **2020**, *379*, 122251.
15. Karges, J.; Kuang, S.; Maschietto, F.; Blacque, O.; Ciofini, I.; Chao, H.; Gasser, G. Rationally Designed Ruthenium Complexes for 1- and 2-photon Photodynamic Therapy. *Nat. Commun.* **2020**, *11* (1), 3262.
16. Yue, W.; Chen, L.; Yu, L.; Zhou, B.; Yin, H.; Ren, W.; Liu, C.; Guo, L.; Zhang, Y.; Sun, L.; Zhang, K.; Xu, H.; Chen, Y. Checkpoint Blockade and Nanosonosensitizer-Augmented Noninvasive Sonodynamic Therapy Combination Reduces Tumour Growth and Metastases in Mice. *Nat. Commun.* **2019**, *10* (1), 2025.
17. Guan, X.; Yin, H. H.; Xu, X. H.; Xu, G.; Zhang, Y.; Zhou, B. G.; Yue, W. W.; Liu, C.; Sun, L. P.; Xu, H. X.; Zhang, K. Tumor Metabolism-Engineered Composite Nanoplatforms Potentiate Sonodynamic Therapy via Reshaping Tumor Microenvironment and Facilitating Electron–Hole Pairs' Separation. *Adv. Funct. Mater.* **2020**, *30* (27), 2000326.
18. Son, S.; Kim, J. H.; Wang, X.; Zhang, C.; Yoon, S. A.; Shin, J.; Sharma, A.; Lee, M. H.; Cheng, L.; Wu, J.; Kim, J. S. Multifunctional Sonosensitizers in Sonodynamic Cancer Therapy. *Chem. Soc. Rev.* **2020**, *49* (11), 3244–3261.
19. Zhu, Y.; Wu, Y.; Li, S.; Yuan, X.; Shen, J.; Luo, S.; Wang, Z.; Gao, R.; Wu, J.; Ge, L. Photocatalytic and Photothermal Bismuthene Nanosheets as Drug Carrier Capable of Generating CO to Improve Drug Sensitivity and Reduce Inflammation for Enhanced Cancer Therapy. *Chem. Eng. J.* **2022**, *446*, 137321.

20. Zheng, D. W.; Li, B.; Li, C. X.; Xu, L.; Fan, J. X.; Lei, Q.; Zhang, X. Z. Photocatalyzing CO2 to CO for Enhanced Cancer Therapy. *Adv. Mater.* **2017**, *29* (44), 1703822.
21. Peng, E.; Wang, F.; Xue, J. M. Nanostructured Magnetic Nanocomposites as MRI Contrast Agents. *J. Mater. Chem. B* **2015**, *3* (11), 2241–2276.
22. Ma, S.; Zhang, J.; Xia, S.; Yin, W.; Qin, Y.; Lei, R.; Kong, J.; Mei, L.; Li, J.; Xin, G.; Li, G. Three-dimensional Angiography Fused with CT/MRI for Multimodal Imaging of Nanoparticles Based on Ba4Yb3F17: Lu(3+),Gd(3+). *Nanoscale* **2018**, *10* (28), 13402–13409.
23. Owens, T. C.; Anton, N.; Attia, M. F. CT and X-Ray Contrast Agents: Current Clinical Challenges and the Future of Contrast. *Acta Biomater.* **2023**, *171*, 19–36.
24. Lusic, H.; Freedman, J. D.; Snyder, B. D.; Grinstaff, M. W. X-Ray Computed Tomography Contrast Agents for Cartilage Imaging. *Abstr. Pap. Am. Chem. S* **2012**, *244*.
25. Lee, N.; Choi, S. H.; Hyeon, T. Nano-Sized CT Contrast Agents. *Adv. Mater.* **2013**, *25* (19), 2641–2660.
26. Zhang, C.; Zhou, L.; Zhang, J.; Dai, R.; Zhuang, P. R.; Ye, Z. X. One-pot Synthesis of Flower-like Bi2S3 Nanoparticles for Spectral CT Imaging and Photothermal Therapy. *New J. Chem.* **2022**, *46* (21), 10458–10469.
27. Dong, L.; Zhang, P.; Liu, X.; Deng, R.; Du, K.; Feng, J.; Zhang, H. Renal Clearable Bi–Bi2S3 Heterostructure Nanoparticles for Targeting Cancer Theranostics. *ACS Appl. Mater. Interfaces* **2019**, *11* (8), 7774–7781.
28. Yu, X. J.; Li, A.; Zhao, C. Z.; Yang, K.; Chen, X. Y.; Li, W. W. Ultrasmall Semimetal Nanoparticles of Bismuth for Dual-Modal Computed Tomography/Photoacoustic Imaging and Synergistic Thermoradiotherapy. *ACS Nano* **2017**, *11* (4), 3990–4001.
29. Zhou, S. M.; Ma, D. K.; Zhang, S. H.; Wang, W.; Chen, W.; Huang, S. M.; Yu, K. PEGylated Cu3BiS3 Hollow Nanospheres as a New Photothermal Agent for 980 Nm-Laser-Driven Photothermochemotherapy and a Contrast Agent for X-Ray Computed Tomography Imaging. *Nanoscale* **2016**, *8* (3), 1374–1382.
30. Zhang, X. L.; Liu, B.; Yao, S.; Liu, Z. M.; Li, J. K. Multifunctional Bi NSs@BSA Nanoplatform Guided by CT Imaging for Effective Photothermal Therapy. *Langmuir* **2022**, *38* (46), 14355–14363.
31. Xu, S.; Wang, J.; Wei, Y.; Zhao, H.; Tao, T.; Wang, H.; Wang, Z.; Du, J.; Wang, H.; Qian, J.; Ma, K.; Wang, J. In Situ One-Pot Synthesis of Fe2O3@BSA Core-Shell Nanoparticles as Enhanced T1-Weighted Magnetic Resonance Imagine Contrast Agents. *ACS Appl. Mater. Interfaces* **2020**, *12* (51), 56701–56711.
32. Wallyn, J.; Anton, N.; Mertz, D.; Begin-Colin, S.; Perton, F.; Serra, C. A.; Franconi, F.; Lemaire, L.; Chiper, M.; Libouban, H.; Messaddeq, N.; Anton, H.; Vandamme, T. F. Magnetite- and Iodine-Containing Nanoemulsion as a Dual Modal Contrast Agent for X-ray/Magnetic Resonance Imaging. *ACS Appl. Mater. Interfaces* **2019**, *11* (1), 403–416.
33. Tong, S.; Zhu, H.; Bao, G. Magnetic Iron Oxide Nanoparticles for Disease Detection and Therapy. *Mater. Today* **2019**, *31*, 86–99.
34. Fernandez-Barahona, I.; Gutierrez, L.; Veintemillas-Verdaguer, S.; Pellico, J.; Morales, M. D. P.; Catala, M.; Del Pozo, M. A.; Ruiz-Cabello, J.; Herranz, F. Cu-Doped Extremely Small Iron Oxide Nanoparticles with Large Longitudinal Relaxivity: One-Pot Synthesis and In Vivo Targeted Molecular Imaging. *ACS Omega* **2019**, *4* (2), 2719–2727.
35. Miao, C.; Hu, F.; Rui, Y.; Duan, Y.; Gu, H. A T1/T2 Dual Functional Iron Oxide MRI Contrast Agent with Super Stability and Low Hypersensitivity Benefited by Ultrahigh Carboxyl Group Density. *J. Mater. Chem. B* **2019**, *7* (12), 2081–2091.
36. Cai, W.; Zhang, Y.; Wang, J.; Wang, Z.; Tian, Y.; Liu, H.; Pan, H.; Fu, L.; Chen, W.; Wu, C.; Wang, X.; Liu, G. Engineering the Surface of Gd2O3 Nanoplates for Improved T1-Weighted Magnetic Resonance Imaging. *Chem. Eng. J.* **2020**, *380*, 122473.
37. Zhu, G.; Chen, L.; Zeng, F.; Gu, L.; Yu, X.; Li, X.; Jiang, J.; Guo, G.; Cao, J.; Tang, K.; Zhu, H.; Daldrup-Link, H. E.; Wu, M. GdVO4:Eu(3+),Bi(3+) Nanoparticles as a Contrast Agent for MRI and Luminescence Bioimaging. *ACS Omega* **2019**, *4* (14), 15806–15814.
38. Park, S. J.; Jang, H. W.; Park, J. Y.; Chung, J. W.; Yang, H. K.; Moon, B. K. Gd2O3:Pr3+ Nanospheres as Bi-functional Contrast Agents for Optical and Magnetic Resonance Imaging Properties. *Ceram. Int.* **2019**, *45* (5), 5958–5964.
39. Liu, C. Y.; Gao, Z. Y.; Zeng, J. F.; Hou, Y.; Fang, F.; Li, Y. L.; Qiao, R. R.; Shen, L.; Lei, H.; Yang, W. S.; Gao, M. Y. Magnetic/Upconversion Fluorescent NaGdF4:Yb,Er Nanoparticle-Based Dual-Modal Molecular Probes for Imaging Tiny Tumors In Vivo. *ACS Nano* **2013**, *7* (8), 7227–7240.
40. Ramasamy, P.; Chandra, P.; Rhee, S. W.; Kim, J. Enhanced Upconversion Luminescence in NaGdF4:Yb,Er Nanocrystals by Fe3+ Doping and Their Application in Bioimaging. *Nanoscale* **2013**, *5* (18), 8711–8717.
41. Wu, X.; Hu, B.; Li, D.; Chen, B.; Huang, Y.; Xie, Z.; Li, L.; Shen, N.; Yang, F.; Shi, W.; Chen, M.; Zhu, Y. Polymer Photocatalysts Containing Segregated π-Conjugation Units with Electron-Trap Activity for Efficient Natural-light-driven Bacterial Inactivation. *Angew. Chem. Int. Ed.* **2023**, *62* (48), e202313787.
42. Fu, Y.; Yang, L.; Zhang, J.; Hu, J.; Duan, G.; Liu, X.; Li, Y.; Gu, Z. Polydopamine Antibacterial Materials. *Mater. Horiz.* **2021**, *8* (6), 1618–1633.
43. Cao, C. Y.; Yang, N.; Zhao, Y.; Yang, D. P.; Hu, Y. L.; Yang, D. L.; Song, X. J.; Wang, W. J.; Dong, X. C. Biodegradable Hydrogel with Thermo-Response and Hemostatic Effect for Photothermal Enhanced Anti-infective Therapy. *Nano Today* **2021**, *39*, 101165.
44. Zou, J. F.; Bao, D. D.; Ma, R.; Zhu, Z. H.; Chen, X. J.; Zhu, J. J.; Fan, X. D.; Zhang, K.; Zheng, H. Y.; Li, F. Z.; Piao, J. G. Green and Sustainable Self-Assembly Nanocomposite from Gentamicin Sulfate/Lignosulfonate with Efficient Antibacterial and Wound-Healing Activity. *ACS Sustain. Chem. Eng.* **2020**, *8* (12), 4931–4940.
45. Li, X.; Wang, B.; Liang, T.; Wang, R.; Song, P.; He, Y. Synthesis of Cationic Acrylate Copolyvidone-Iodine Nanoparticles with Double Active Centers and Their Antibacterial Application. *Nanoscale* **2020**, *12* (42), 21940–21950.
46. Zhao, Q.; Zhao, Y.; Lu, Z.; Tang, Y. Amino Acid-Modified Conjugated Oligomer Self-Assembly Hydrogel for Efficient Capture and Specific Killing of Antibiotic-Resistant Bacteria. *ACS Appl. Mater. Interfaces* **2019**, *11* (18), 16320–16327.
47. Zheng, L.; Li, J.; Yu, M.; Jia, W.; Duan, S.; Cao, D.; Ding, X.; Yu, B.; Zhang, X.; Xu, F. J. Molecular Sizes and Antibacterial Performance Relationships of Flexible Ionic Liquid Derivatives. *J. Am. Chem. Soc.* **2020**, *142* (47), 20257–20269.
48. Zhang, T.; Yu, H.; Li, J.; Song, H.; Wang, S.; Zhang, Z.; Chen, S. Green Light–Triggered Antimicrobial Cotton Fabric for Wastewater Disinfection. *Mater. Today Phys.* **2020**, *15*, 100254.
49. Zhang, D.; Liu, H. M.; Shu, X.; Feng, J.; Yang, P.; Dong, P.; Xie, X.; Shi, Q. Nanocopper-loaded Black Phosphorus Nanocomposites for Efficient Synergistic Antibacterial Application. *J. Hazard Mater.* **2020**, *393*, 122317.
50. Çekceoglu, I. A.; Eroglu, Z.; Küçükkeçeci, H.; Sevgi, F.; Ersoz, M.; Patir, I. H.; Metin, Ö. A NIR-Light-Driven Black Phosphorus Based Nanocomposite for Combating Bacteria. *ChemistrySelect* **2022**, *7* (6), e202104137.
51. Wu, Q.; Liu, X. M.; Li, B.; Tan, L.; Han, Y.; Li, Z. Y.; Liang, Y. Q.; Cui, Z. D.; Zhu, S. L.; Wu, S. L.; Zheng, Y. F. Eco-friendly and Degradable Red

Phosphorus Nanoparticles for Rapid Microbial Sterilization under Visible Light. *J. Mater. Sci. Technol.* **2021**, *67*, 70–79.
52. Ran, P.; Chen, W. J.; Zheng, H.; Zhou, J. J.; Qiu, B.; Cao, W. X.; Li, X. H. Surface Decoration of Black Phosphorus Nanosheets to Generate Oxygen and Release O for Photodynamic Killing of Bacteria. *Nanoscale* **2021**, *13* (31), 13506–13518.
53. Feng, Y.; Chen, H.; Shao, B.; Zhao, S.; Wang, Z.; You, H. Renal-Clearable Peptide-Functionalized Ba2GdF7 Nanoparticles for Positive Tumor-Targeting Dual-Mode Bioimaging. *ACS Appl. Mater. Interfaces* **2018**, *10* (30), 25511–25518.
54. Chen, X.; Shi, S.; Wei, J.; Chen, M.; Zheng, N. Two-dimensional Pd-Based Nanomaterials for Bioapplications. *Sci. Bull.* **2017**, *62* (8), 579–588.
55. Xu, J.; Chen, X.; Xu, Y.; Du, Y.; Yan, C. Ultrathin 2D Rare-Earth Nanomaterials: Compositions, Syntheses, and Applications. *Adv. Mater.* **2019**, e1806461; https://doi.org/10.1002/adma.201806461.
56. Yuan, E.; Si, P.; Winetraub, Y.; Shevidi, S.; de la Zerda, A. A Spectral Demixing Model for Triplex In Vivo Imaging of Optical Coherence Tomography Contrast Agents. *ACS Photonics* **2020**, *7* (4), 893–900.
57. Wang, H.; Revia, R.; Mu, Q.; Lin, G.; Yen, C.; Zhang, M. Single-layer Boron-Doped Graphene Quantum Dots for Contrast-Enhanced In Vivo T1-Weighted MRI. *Nanoscale Horiz.* **2020**, *5* (3), 573–579.
58. Tan, L.; He, C.; Chu, X.; Chu, Y.; Ding, Y. Charge-reversal ZnO-Based Nanospheres for Stimuli-Responsive Release of Multiple Agents towards Synergistic Cancer Therapy. *Chem. Eng. J.* **2020**, *395*, 125177.
59. Naha, P. C.; Hsu, J. C.; Kim, J.; Shah, S.; Bouche, M.; Si-Mohamed, S.; Rosario-Berrios, D. N.; Douek, P.; Hajfathalian, M.; Yasini, P.; Singh, S.; Rosen, M. A.; Morgan, M. A.; Cormode, D. P. Dextran-Coated Cerium Oxide Nanoparticles: A Computed Tomography Contrast Agent for Imaging the Gastrointestinal Tract and Inflammatory Bowel Disease. *ACS Nano* **2020**, *14* (8), 10187–10197.
60. Hosseini, M.; Ahmadi, Z.; Khoobi, M.; Dehghani, S.; Kefayat, A. High-Performance Spirulina–Bismuth Biohybrids for Enhanced Computed Tomography Imaging. *ACS Sustain. Chem. Eng.* **2020**, *8* (34), 13085–13099.
61. Zhang, J.; Yuan, Y.; Gao, M.; Han, Z.; Chu, C.; Li, Y.; van Zijl, P. C. M.; Ying, M.; Bulte, J. W. M.; Liu, G. Carbon Dots as a New Class of Diamagnetic Chemical Exchange Saturation Transfer (diaCEST) MRI Contrast Agents. *Angew Chem. Int. Ed. Engl.* **2019**, *58* (29), 9871–9875.
62. Lu, C.; Dong, P.; Pi, L.; Wang, Z.; Yuan, H.; Liang, H.; Ma, D.; Chai, K. Y. Hydroxyl-PEG-Phosphonic Acid-Stabilized Superparamagnetic Manganese Oxide-Doped Iron Oxide Nanoparticles with Synergistic Effects for Dual-Mode MR Imaging. *Langmuir* **2019**, *35* (29), 9474–9482.
63. Li, Y.; Zeng, S.; Hao, J. Non-Invasive Optical Guided Tumor Metastasis/Vessel Imaging by Using Lanthanide Nanoprobe with Enhanced Down-Shifting Emission beyond 1500 Nm. *ACS Nano* **2019**, *13* (1), 248–259.
64. Xu, R.; Xu, Z.; Si, Y.; Xing, X.; Li, Q.; Xiao, J.; Wang, B.; Tian, G.; Zhu, L.; Wu, Z.; Zhang, G. Oxygen Vacancy Defect-Induced Activity Enhancement of Gd Doping Magnetic Nanocluster for Oxygen Supplying Cancer Theranostics. *ACS Appl. Mater. Interfaces* **2020**, *12* (33), 36917–36927.
65. Xiao, S. T.; Lu, Y.; Feng, M.; Dong, M.; Cao, Z.; Zhang, X. G.; Chen, Y.; Liu, J. Multifunctional FeS2 Theranostic Nanoparticles for Photothermal-Enhanced Chemodynamic/photodynamic Cancer Therapy and Photoacoustic Imaging. *Chem. Eng. J.* **2020**, *396*, 125294.
66. Wang, X.; Zhong, X.; Bai, L.; Xu, J.; Gong, F.; Dong, Z.; Yang, Z.; Zeng, Z.; Liu, Z.; Cheng, L. Ultrafine Titanium Monoxide (TiO1+x) Nanorods for Enhanced Sonodynamic Therapy. *J. Am. Chem. Soc.* **2020**, *142* (14), 6527–6537.
67. Wang, L.; Xu, S. M.; Yang, X.; He, S.; Guan, S.; Waterhouse, G. I. N.; Zhou, S. Exploiting Co Defects in CoFe-Layered Double Hydroxide (CoFe-LDH) Derivatives for Highly Efficient Photothermal Cancer Therapy. *ACS Appl. Mater. Interfaces* **2020**, *12* (49), 54916–54926.
68. Wang, H.; Bremner, D. H.; Wu, K.; Gong, X.; Fan, Q.; Xie, X.; Zhang, H.; Wu, J.; Zhu, L.-M. Platelet Membrane Biomimetic Bufalin-Loaded Hollow MnO2 Nanoparticles for MRI-Guided Chemo-Chemodynamic Combined Therapy of Cancer. *Chem. Eng. J.* **2020**, *382*, 122848.
69. Wang, D.; Tang, M. C.; Jiang, H. J.; Li, M. H.; Jiang, S.; Sun, L.; Sun, J. B. Helical Bowl-like SnS2 with Structure-Induced Conversion Efficiency for Enhanced Photothermal Therapy. *Chem. Eng. J.* **2020**, *400*, 125814.
70. Li, M.; Lin, H.; Qu, F. FeS2@C-ICG-PEG Nanostructure with Intracellular O2 Generation for Enhanced Photo-Dynamic/thermal Therapy and Imaging. *Chem. Eng. J.* **2020**, *384*, 123374.
71. Dai, C.; Hu, R.; Wang, C.; Liu, Z.; Zhang, S.; Yu, L.; Chen, Y.; Zhang, B. Defect Engineering of 2D BiOCl Nanosheets for Photonic Tumor Ablation. *Nanoscale Horiz.* **2020**, *5* (5), 857–868.
72. Yuan, M.; Xu, S.; Zhang, Q.; Zhao, B.; Feng, B.; Ji, K.; Yu, L.; Chen, W.; Hou, M.; Xu, Y.; Fu, X. Bicompatible Porous Co3O4 Nanoplates with Intrinsic Tumor Metastasis Inhibition for Multimodal Imaging and DNA Damage–Mediated Tumor Synergetic Photothermal/photodynamic Therapy. *Chem. Eng. J.* **2020**, *394*, 124874.
73. Cui, Z. M.; Yang, H.; Wang, B.; Li, R. S.; Wang, X. X. Effect of Experimental Parameters on the Hydrothermal Synthesis of Bi2WO6 Nanostructures. *Nanoscale Res. Lett.* **2016**, *11*, 190.
74. Dharmaiah, P.; Lee, C. H.; Madavali, B.; Hong, S. J. Effect of Surfactant Addition on Bi2Te3 Nanostructures Synthesized by Hydrothermal Method. *Arch. Metall. Mater.* **2017**, *62* (2), 1005–1010.
75. Si, Y.; Zhang, G.; Wang, D.; Zhang, C.; Yang, C.; Bai, G.; Qian, J.; Chen, Q.; Zhang, Z.; Wu, Z.; Xu, Y.; Zou, D. Nanostructure-enhanced Water Interaction to Increase the Dual-Mode MR Contrast Performance of Gadolinium-Doped Iron Oxide Nanoclusters. *Chem. Eng. J.* **2019**, *360*, 289–298.
76. Ma, S.; Kong, J.; Luo, X.; Xie, J.; Zhou, Z.; Bai, X. Recent Progress on Bismuth-Based Light-Triggered Antibacterial Nanocomposites: Synthesis, Characterization, Optical Properties and Bactericidal Applications. *Sci. Total Environ.* **2024**, *915*, 170125.
77. Wang, X. Y.; Zhang, F. C.; Yang, Y. N.; Shao, T. T.; Zhang, S. L.; Zhou, B. S. Microwave Method Synthesis and Photocatalytic Activity of Nano-BiOBr Photocatalyst. *Ferroelectrics* **2020**, *564* (1), 70–77.
78. Miao, Y. C.; Lian, Z. C.; Huo, Y. N.; Li, H. X. Microwave-assisted Ionothermal Synthesis of Hierarchical Microcube-like BiOBr with Enhanced Photocatalytic Activity. *Chin. J. Catal.* **2018**, *39* (8), 1411–1417.
79. Zhu, X. H.; Hang, Q. M.; Xing, Z. B.; Yang, Y.; Zhu, J. M.; Liu, Z. G.; Ming, N. B.; Zhou, P.; Song, Y.; Li, Z. S.; Yu, T.; Zou, Z. G. Microwave Hydrothermal Synthesis, Structural Characterization, and Visible-Light Photocatalytic Activities of Single-Crystalline Bismuth Ferric Nanocrystals. *J. Am. Ceram. Soc.* **2011**, *94* (8), 2688–2693.
80. Yu, H.; Hu, M.; Chen, C.; Hu, C.; Li, Q.; Hu, F.; Peng, S.; Ma, J. Ambient γ-Rays-Mediated Noble-Metal Deposition on Defect-Rich Manganese Oxide for Glycerol-Assisted H2 Evolution at Industrial-Level Current Density. *Angew. Chem. Int. Ed.* **2023**, *62* (52), e202314569.
81. Zhang, M. X.; Yuan, M. J.; Zhao, X. F.; Chen, J. C.; He, L. W.; Gao, Q. H.; Hu, J. T.; Wu, G. Z.; Chai, Z. F.; Wang, S. A. Radiation-induced One-Pot Synthesis of Grafted Covalent Organic Frameworks. *Sci. China Chem.* **2023**, *66* (6), 1781–1787.
82. Ahmad, S.; Hammad, R.; Rubab, S. Gamma Radiation-Induced Synthesis of Polyaniline-Based Nanoparticles/Nanocomposites. *J. Electron. Mater.* **2022**, *51* (10), 5550–5567.

83. Chen, J.; Zhang, M.; Shu, J.; Yuan, M.; Yan, W.; Bai, P.; He, L.; Shen, N.; Gong, S.; Zhang, D.; Li, J.; Hu, J.; Li, R.; Wu, G.; Chai, Z.; Yu, J.; Wang, S. Electron Beam Irradiation-Induced Formation of Defect-Rich Zeolites under Ambient Condition within Minutes. *Angew Chem. Int. Ed. Engl.* **2021**, *60* (27), 14858–14863.
84. Maleki, H. Photocatalytic Activity, Optical and Ferroelectric Properties of Bi0.8Nd0.2FeO3 Nanoparticles Synthesized by Sol-Gel and Hydrothermal Methods. *J. Magn. Magn. Mater.* **2018**, *458*, 277–284.
85. Zhang, Q.; Sando, D.; Nagarajan, V. Chemical Route Derived Bismuth Ferrite Thin Films and Nanomaterials. *J. Mater. Chem. C* **2016**, *4* (19), 4092–4124.
86. Cao, X. Q.; Gu, Y.; Tian, H. L.; Fang, Y. F.; Johnson, D.; Ren, Z. Y.; Chen, C. C.; Huang, Y. P. Microemulsion Synthesis of Ms/tz-BiVO4 Composites: The Effect of pH on Crystal Structure and Photocatalytic Performance. *Ceram. Int.* **2020**, *46* (13), 20788–20797.
87. Long, D.; Liu, J.; Bai, L.; Yan, L.; Liu, H.; Feng, Z.; Zheng, L.; Chen, X.; Li, S.; Lu, M. Continuously Selective Photocatalytic CO2 Fixation via Controllable S/Se Ratio in a TiO2–MoSxSey Dual-Excitation Heterostructured Nanotree. *ACS Photonics* **2020**, *7* (12), 3394–3400.
88. Barge, A.; Baricco, F.; Cravotto, G.; Fretta, R.; Lattuada, L. Mechanochemistry Applied to the Synthesis of X-Ray Contrast Agent. *ACS Sustain. Chem. Eng.* **2020**, *8* (34), 12825–12830.
89. Zhang, R.; Xu, Y.; Zhang, Y.; Kim, H. S.; Sharma, A.; Gao, J.; Yang, G.; Kim, J. S.; Sun, Y. Rational Design of a Multifunctional Molecular Dye for Dual-Modal NIR-II/photoacoustic Imaging and Photothermal Therapy. *Chem. Sci.* **2019**, *10* (36), 8348–8353.
90. Xiong, Y.; Sun, F.; Liu, P.; Yang, Z.; Cao, J.; Liu, H.; Liu, P.; Hu, J.; Xu, Z.; Yang, S. A Biomimetic One-Pot Synthesis of Versatile Bi2S3/FeS2 Theranostic Nanohybrids for Tumor-Targeted Photothermal Therapy Guided by CT/MR Dual-Modal Imaging. *Chem. Eng. J.* **2019**, *378*, 122172.
91. Wang, L.; Guan, S.; Weng, Y.; Xu, S. M.; Lu, H.; Meng, X.; Zhou, S. Highly Efficient Vacancy-Driven Photothermal Therapy Mediated by Ultrathin MnO2 Nanosheets. *ACS Appl. Mater. Interfaces* **2019**, *11* (6), 6267–6275.
92. Gao, Y.; Wang, F.; Huang, W.; Yang, C.; Guo, W.; Song, C.; Zhang, Q.; Yang, B.; Xu, Y.; Guo, C. SnxWO3 as a Theranostic Platform for Realizing Multi-Imaging-Guided Photothermal/photodynamic Combination Therapy. *Nanoscale* **2019**, *11* (7), 3300–3310.
93. Meng, X.; Liu, Z.; Cao, Y.; Dai, W.; Zhang, K.; Dong, H.; Feng, X.; Zhang, X. Fabricating Aptamer-Conjugated PEGylated-MoS2/Cu1.8S Theranostic Nanoplatform for Multiplexed Imaging Diagnosis and Chemo-Photothermal Therapy of Cancer. *Adv. Funct. Mater.* **2017**, *27* (16), 1605592.
94. Yang, N.; Xiao, W.; Song, X.; Wang, W.; Dong, X. Recent Advances in Tumor Microenvironment Hydrogen Peroxide-Responsive Materials for Cancer Photodynamic Therapy. *Nano-Micro Lett.* **2020**, *12* (1), 15.
95. Zhou, R.; Yan, L.; Dong, X.; Zhu, S.; Chen, K.; Wu, Y.; Xiang, H.; Li, L.; Zhang, G.; Gu, Z.; Zhao, Y. Fractionated Regimen-Suitable Immunoradiotherapy Sensitizer Based on Ultrasmall Fe4Se2W18 Nanoclusters Enable Tumor-specific Radiosensitization Augment and Antitumor Immunity Boost. *Nano Today* **2021**, *36*, 101003.
96. Song, G.; Cheng, L.; Chao, Y.; Yang, K.; Liu, Z. Emerging Nanotechnology and Advanced Materials for Cancer Radiation Therapy. *Adv. Mater.* **2017**, *29* (32), 1700996.
97. An, J.; Hu, Y. G.; Li, C.; Hou, X. L.; Cheng, K.; Zhang, B.; Zhang, R. Y.; Li, D. Y.; Liu, S. J.; Liu, B.; Zhu, D.; Zhao, Y. D. A pH/Ultrasound Dual-Response Biomimetic Nanoplatform for Nitric Oxide Gas-Sonodynamic Combined Therapy and Repeated Ultrasound for Relieving Hypoxia. *Biomaterials* **2020**, *230*, 119636.
98. Wang, Y. M.; Feng, W.; Chang, M. Q.; Yang, J. C.; Guo, Y. D.; Ding, L.; Yu, L. D.; Huang, H.; Chen, Y.; Shi, J. L. Engineering 2D Multifunctional Ultrathin Bismuthene for Multiple Photonic Nanomedicine. *Adv. Funct. Mater.* **2021**, *31* (6), 2005093.
99. Ma, S.; Xie, J.; Wang, L.; Zhou, Z.; Luo, X.; Yan, J.; Ran, G. Hetero-Core-Shell BiNS-Fe@Fe as a Potential Theranostic Nanoplatform for Multimodal Imaging-Guided Simultaneous Photothermal-Photodynamic and Chemodynamic Treatment. *ACS Appl. Mater. Interfaces* **2021**, *13* (9), 10728–10740.
100. Zhang, Q.; Wang, W.; Zhang, M.; Wu, F.; Zheng, T.; Sheng, B.; Liu, Y.; Shen, J.; Zhou, N.; Sun, Y. A Theranostic Nanocomposite with Integrated Black Phosphorus Nanosheet, Fe3O4@MnO2-Doped Upconversion Nanoparticles and Chlorin for Simultaneous Multimodal Imaging, Highly Efficient Photodynamic and Photothermal Therapy. *Chem. Eng. J.* **2020**, *391*, 123525.
101. Lv, K.; Lin, H.; Qu, F. Biodegradable Hollow Co3S4@N-Doped Carbon as Enhanced PTT/PDT Agent for Multimodal MR/thermal Imaging and Synergistic Antitumor Therapy. *Chem. Eng. J.* **2020**, *392*, 124555.
102. Zhang, F.; Liu, Y.; Lei, J.; Wang, S.; Ji, X.; Liu, H.; Yang, Q. Metal-Organic-Framework-Derived Carbon Nanostructures for Site-specific Dual-Modality Photothermal/Photodynamic Thrombus Therapy. *Adv. Sci.* **2019**, *6* (17), 1901378.
103. Guan, Q.; Zhou, L. L.; Li, Y. A.; Li, W. Y.; Wang, S.; Song, C.; Dong, Y. B. Nanoscale Covalent Organic Framework for Combinatorial Antitumor Photodynamic and Photothermal Therapy. *ACS Nano* **2019**, *13* (11), 13304–13316.
104. Cheng, Y.; Chang, Y.; Feng, Y.; Jian, H.; Wu, X.; Zheng, R.; Xu, K.; Zhang, H. Bismuth Sulfide Nanorods with Retractable Zinc Protoporphyrin Molecules for Suppressing Innate Antioxidant Defense System and Strengthening Phototherapeutic Effects. *Adv. Mater.* **2019**, *31* (10), e1806808.
105. Huang, X. Y.; Zha, F. J.; Zou, J. H.; Li, Y. X.; Wang, F.; Chen, X. Y. Photoacoustic Imaging-Guided Synergistic Photothermal/ Radiotherapy Using Plasmonic Bi/BiO Nanoparticles. *Adv. Funct. Mater.* **2022**, *32* (23), 2113353.
106. Chang, Y. F.; Bai, Q. C.; Wang, M.; Ma, Y. J.; Yu, K.; Lu, H. Q.; Lu, T.; Lin, H. M.; Qu, F. Y. Plasmonic Bi Nanoparticles Encapsulated by N-Carbon for Dual-Imaging and Photothermal/photodynamic/chemo-Therapy. *Biomater. Adv.* **2022**, *134*, 112546.
107. Peng, X.; Pan, Q.; Li, J.; Zhu, W.; Zhang, N.; Pu, Y.; Luo, K.; He, B. Polymer-directed Supramolecular Assembly of Photosensitizers: Evocation of Photothermal Effect and Highly Efficient Loading of Disulfiram for Chemo-Phototherapy of Cancer. *Appl. Mater. Today* **2021**, *22*, 100931.
108. Liu, C.; Zhang, L.; Chen, X.; Li, S.; Han, Q.; Li, L.; Wang, C. Biomolecules-assisted Synthesis of Degradable Bismuth Nanoparticles for Dual-Modal Imaging-Guided Chemo-Photothermal Therapy. *Chem. Eng. J.* **2020**, *382*, 122720.
109. Zhu, W.; Chen, M.; Liu, Y.; Tian, Y.; Song, Z.; Song, G.; Zhang, X. A Dual Factor Activated Metal-Organic Framework Hybrid Nanoplatform for Photoacoustic Imaging and Synergetic Photo-Chemotherapy. *Nanoscale* **2019**, *11*, 20630–20637.
110. Yang, Y.; Deng, Y.; Huang, J.; Fan, X.; Cheng, C.; Nie, C.; Ma, L.; Zhao, W.; Zhao, C. Size-Transformable Metal–Organic Framework–Derived

Nanocarbons for Localized Chemo-Photothermal Bacterial Ablation and Wound Disinfection. *Adv. Funct. Mater.* **2019**, *29* (33), 1900143.
111. Avellini, T.; Soni, N.; Silvestri, N.; Fiorito, S.; De Donato, F.; De Mei, C.; Walther, M.; Cassani, M.; Ghosh, S.; Manna, L.; Stephan, H.; Pellegrino, T. Cation Exchange Protocols to Radiolabel Aqueous Stabilized ZnS, ZnSe, and CuFeS2 Nanocrystals with (64)Cu for Dual Radio- and Photo-Thermal Therapy. *Adv. Funct. Mater.* **2020**, *30* (28), 2002362.
112. Malehmir, S.; Abedini, A.; Sobhani-Nasab, A.; Eshraghi, R.; Akbari, M.; Atapour, A.; Hasan-Abad, A. M. A Review of Biogenic Routes for the Manufacture of Manganese Oxide Nanostructures and its Anti-cancer, Drug Delivery, Anti-bacterial, and Bioimaging Potentials. *Inorg. Chem. Commun.* **2023**, *156*, 111306.
113. Le, N. A.; Kuo, W.; Muller, B.; Kurtcuoglu, V.; Spingler, B. Crosslinkable Polymeric Contrast Agent for High-Resolution X-Ray Imaging of the Vascular System. *Chem. Commun.* **2020**, *56* (44), 5885–5888.
114. Cai, Y.; Wang, Y.; Xu, H.; Cao, C.; Zhu, R.; Tang, X.; Zhang, T.; Pan, Y. Positive Magnetic Resonance Angiography Using Ultrafine Ferritin-Based Iron Oxide Nanoparticles. *Nanoscale* **2019**, *11* (6), 2644–2654.
115. Piche, D.; Tavernaro, I.; Fleddermann, J.; Lozano, J. G.; Varambhia, A.; Maguire, M. L.; Koch, M.; Ukai, T.; Hernandez Rodriguez, A. J.; Jones, L.; Dillon, F.; Reyes Molina, I.; Mitzutani, M.; Gonzalez Dalmau, E. R.; Maekawa, T.; Nellist, P. D.; Kraegeloh, A.; Grobert, N. Targeted T1 Magnetic Resonance Imaging Contrast Enhancement with Extraordinarily Small CoFe2O4 Nanoparticles. *ACS Appl. Mater. Interfaces* **2019**, *11* (7), 6724–6740.
116. Yang, L.; Wang, Z.; Ma, L.; Li, A.; Xin, J.; Wei, R.; Lin, H.; Wang, R.; Chen, Z.; Gao, J. The Roles of Morphology on the Relaxation Rates of Magnetic Nanoparticles. *ACS Nano* **2018**, *12* (5), 4605–4614.
117. Wei, R.; Cai, Z.; Ren, B. W.; Li, A.; Lin, H.; Zhang, K.; Chen, H.; Shan, H.; Ai, H.; Gao, J. Biodegradable and Renal-Clearable Hollow Porous Iron Oxide Nanoboxes for In Vivo Imaging. *Chem. Mater.* **2018**, *30* (21), 7950–7961.
118. Feng, Y.; Chen, H.; Ma, L.; Shao, B.; Zhao, S.; Wang, Z.; You, H. Surfactant-Free Aqueous Synthesis of Novel Ba2GdF7:Yb(3+), Er(3+) @PEG Upconversion Nanoparticles for In Vivo Trimodality Imaging. *ACS Appl. Mater. Interfaces* **2017**, *9* (17), 15096–15102.
119. Wang, Y.; Xu, C.; Chang, Y.; Zhao, L.; Zhang, K.; Zhao, Y.; Gao, F.; Gao, X. Ultrasmall Superparamagnetic Iron Oxide Nanoparticle for T2-Weighted Magnetic Resonance Imaging. *ACS Appl. Mater. Interfaces* **2017**, *9* (34), 28959–28966.
120. Liu, F. Y.; He, X. X.; Liu, L.; You, H. P.; Zhang, H. M.; Wang, Z. X. Conjugation of NaGdF4 Upconverting Nanoparticles on Silica Nanospheres as Contrast Agents for Multi-Modality Imaging. *Biomaterials* **2013**, *34* (21), 5218–5225.
121. Hong, C.; Liu, Z.; Mao, Q.; Zheng, J.; Sun, Y.; Lv, Y.; Wang, P.; Wu, M.; Lin, J.; Gao, C.; Ma, X.; Pan, Y.; Zhang, J.; Chen, T.; Yang, X.; Wu, A. Oxygen-defect Bismuth Oxychloride Nanosheets for Ultrasonic Cavitation Effect Enhanced Sonodynamic and Second Near-Infrared Photo-Induced Therapy of Breast Cancer. *Biomaterials* **2025**, *312*, 122709.
122. Chu, B.; Chen, Z.; Wu, X.; Shi, H.; Jin, X.; Song, B.; Cui, M.; Zhao, Y.; Zhao, Y.; He, Y.; Wang, H.; Dong, F. Photoactivated Gas-Generating Nanocontrast Agents for Long-Term Ultrasonic Imaging-Guided Combined Therapy of Tumors. *ACS Nano* **2024**, *18* (24), 15590–15606.
123. Guo, Y.; Li, Y.; Yang, Y.; Tang, S.; Zhang, Y.; Xiong, L. Multiscale Imaging of Brown Adipose Tissue in Living Mice/Rats with Fluorescent Polymer Dots. *ACS Appl. Mater. Interfaces* **2018**, *10* (24), 20884–20896.
124. Su, Y.; Huang, L.; Zhang, D.; Zeng, Z.; Hong, S.; Lin, X. Recent Advancements in Ultrasound Contrast Agents Based on Nanomaterials for Imaging. *ACS Biomater. Sci. Eng.* **2024**, *10* (9), 5496–5512.
125. Lobatto, M. E.; Binderup, T.; Robson, P. M.; Giesen, L. F. P.; Calcagno, C.; Witjes, J.; Fay, F.; Baxter, S.; Wessel, C. H.; Eldib, M.; Bini, J.; Carlin, S. D.; Stroes, E. S. G.; Storm, G.; Kjaer, A.; Lewis, J. S.; Reiner, T.; Fayad, Z. A.; Mulder, W. J. M.; Perez-Medina, C. Multimodal Positron Emission Tomography Imaging to Quantify Uptake of (89)Zr-Labeled Liposomes in the Atherosclerotic Vessel Wall. *Bioconjug. Chem.* **2019**, *31*, 360–368.
126. Si, P.; Yuan, E.; Liba, O.; Winetraub, Y.; Yousefi, S.; SoRelle, E. D.; Yecies, D. W.; Dutta, R.; de la Zerda, A. Gold Nanoprisms as Optical Coherence Tomography Contrast Agents in the Second Near-Infrared Window for Enhanced Angiography in Live Animals. *ACS Nano* **2018**, *12* (12), 11986–11994.
127. He, S.; Johnson, N. J. J.; Nguyen Huu, V. A.; Cory, E.; Huang, Y.; Sah, R. L.; Jokerst, J. V.; Almutairi, A. Simultaneous Enhancement of Photoluminescence, MRI Relaxivity, and CT Contrast by Tuning the Interfacial Layer of Lanthanide Heteroepitaxial Nanoparticles. *Nano Lett.* **2017**, *17* (8), 4873–4880.
128. Yu, E. Y.; Chandrasekharan, P.; Berzon, R.; Tay, Z. W.; Zhou, X. Y.; Khandhar, A. P.; Ferguson, R. M.; Kemp, S. J.; Zheng, B.; Goodwill, P. W.; Wendland, M. F.; Krishnan, K. M.; Behr, S.; Carter, J.; Conolly, S. M. Magnetic Particle Imaging for Highly Sensitive, Quantitative, and Safe In Vivo Gut Bleed Detection in a Murine Model. *ACS Nano* **2017**, *11* (12), 12067–12076.
129. Ma, S.; Li, X.; Kong, J.; Yu, X.; Bai, X. Light-triggered Bactericidal Semiconductor Nanomaterials: Classification, Modification and Antibacterial Strategies. *Appl. Mater. Today* **2024**, *39*, 102279.
130. Hussain, A.; Hou, J.; Tahir, M.; Ali, S. S.; Rehman, Z. U.; Bilal, M.; Zhang, T.; Dou, Q.; Wang, X. Recent Advances in BiOX-Based Photocatalysts to Enhanced Efficiency for Energy and Environment Applications. *Catal. Rev.* **2022**, 1–55; https://doi.org/10.1080/01614940.2022.2041836.
131. Ma, S.; Luo, X.; Ran, G.; Li, Y.; Cao, Z.; Liu, X.; Chen, G.; Yan, J.; Wang, L. Defect Engineering of Ultrathin 2D Nanosheet BiOI/Bi for Enhanced Photothermal-Catalytic Synergistic Bacteria-Killing. *Chem. Eng. J.* **2022**, *435*, 134810.
132. Wang, Y.; Huang, W.; Guo, S.; Xin, X.; Zhang, Y.; Guo, P.; Tang, S.; Li, X. Sulfur-Deficient ZnIn2S4/Oxygen-Deficient WO3 Hybrids with Carbon Layer Bridges as a Novel Photothermal/Photocatalytic Integrated System for Z-Scheme Overall Water Splitting. *Adv. Energy Mater.* **2021**, *11* (46), 2102452.
133. Pei, L.; Wang, X.; Zhu, H.; Yu, H.; Bandaru, S.; Yan, S.; Zou, Z. Photothermal Effect- and Interfacial Chemical Bond-Modulated NiOx/Ta3N5 Heterojunction for Efficient CO2 Photoreduction. *ACS Appl. Mater. Interfaces* **2023**, *15* (44), 51300–51308.
134. Ma, S.; Wang, L.; Liu, Z.; Luo, X.; Zhou, Z.; Xie, J.; Li, Y.; Cong, S.; Zhou, M.; Xu, Y.; Ran, G. One Stone, Two Birds": Engineering 2-D Ultrathin Heterostructure Nanosheet BiNS@NaLnF4 for Dual-Modal Computed Tomography/magnetic Resonance Imaging Guided, Photonic Synergetic Theranostics. *Nanoscale* **2021**, *13* (1), 185–194.
135. Sun, J.; Wen, J.; Wu, G.; Zhang, Z.; Chen, X.; Wang, G.; Liu, M. Harmonizing the Electronic Structures on BiOI with Active Oxygen Vacancies toward Facet-dependent Antibacterial Photodynamic Therapy. *Adv. Funct. Mater.* **2020**, *30* (42), 2004108.
136. Li, J.; Liu, X.; Tan, L.; Cui, Z.; Yang, X.; Liang, Y.; Li, Z.; Zhu, S.; Zheng, Y.; Yeung, K. W. K.; Wang, X.; Wu, S. Zinc-doped Prussian Blue Enhances Photothermal Clearance of *Staphylococcus aureus* and Promotes Tissue Repair in Infected Wounds. *Nat. Commun.* **2019**, *10* (1), 4490.

137. Ma, H.; He, Y.; Chen, P.; Wang, H.; Sun, Y. J.; Li, J. Y.; Dong, F.; Xie, G. X.; Sheng, J. P. Ultrathin Two-Dimensional Bi-based Photocatalysts: Synthetic Strategies, Surface Defects, and Reaction Mechanisms. *Chem. Eng. J.* **2021**, *417*, 129305.
138. Zeng, W.; Li, J.; Feng, L. P.; Pan, H. X.; Zhang, X. D.; Sun, H. Q.; Liu, Z. T. Synthesis of Large-Area Atomically Thin BiOI Crystals with Highly Sensitive and Controllable Photodetection. *Adv. Funct. Mater.* **2019**, *29* (16), 1900129.
139. Meng, N. Q.; Xu, P. J.; Wen, C. C.; Liu, H. H.; Gao, C. J.; Shen, X. C.; Liang, H. Near-infrared-II-activatable Sulfur-Deficient Plasmonic Bi2S3-X-Au Heterostructures for Photoacoustic Imaging-Guided Ultrasound Enhanced High Performance Phototherapy. *J. Colloid Interface Sci.* **2023**, *644*, 437–453.
140. Wu, X.; Ling Tan, H.; Zhang, C.; Teng, Z.; Liu, Z.; Hau Ng, Y.; Zhang, Q.; Su, C. Recent Advances in Two-Dimensional Ultrathin Bi-based Photocatalysts. *Prog. Mater. Sci.* **2023**, *133*; https://doi.org/10.1016/j.pmatsci.2022.101047.
141. Yougbare, S.; Chou, H. L.; Yang, C. H.; Krisnawati, D. I.; Jazidie, A.; Nuh, M.; Kuo, T. R. Facet-dependent Gold Nanocrystals for Effective Photothermal Killing of Bacteria. *J. Hazard Mater.* **2021**, *407*, 124617.
142. Li, M.; Yu, S. X.; Huang, H. W.; Li, X. W.; Feng, Y. B.; Wang, C.; Wang, Y. G.; Ma, T. Y.; Guo, L.; Zhang, Y. H. Unprecedented Eighteen-Faceted BiOCl with a Ternary Facet Junction Boosting Cascade Charge Flow and Photo-Redox. *Angew. Chem. Int. Ed.* **2019**, *58* (28), 9517–9521.
143. Wu, H.; Li, L.; Wang, S.; Zhu, N.; Li, Z.; Zhao, L.; Wang, Y. Recent Advances of Semiconductor Photocatalysis for Water Pollutant Treatment: Mechanisms, Materials and Applications. *Phys. Chem. Chem. Phys.* **2023**, *25* (38), 25899–25924.